

Freeze-in and Freeze-out of Dark Matter with Charged Long-lived Partners

Sreemanti Chakraborti,^a Victoria Martin^b and Poulose Poulose^a

^aDepartment of Physics, Indian Institute of Technology Guwahati, Assam 781039, India

^bSchool of Physics and Astronomy, University of Edinburgh, Edinburgh

E-mail: sreemanti@iitg.ac.in, victoria.martin@ed.ac.uk, poulose@iitg.ac.in

Abstract. We present a novel framework capable of addressing the dark matter problem through freeze-in and freeze-out mechanisms, separately or together, depending on the region of the parameter space considered. In the dark matter dynamics, the model features an interplay of thermal production along with sizeable contribution through feeble decay of associated dark fermionic partner, which finally freezes out to the right relic density for a wide range of masses and couplings. Apart from the fermionic dark matter candidate, the model introduces two charged partners, one fermionic and another scalar, which often have delayed decays leading to distinct characteristics of such long-lived particles (LLP) in the colliders like the LHC. Our analysis shows that within the present scenario, LLP of decay length that could be probed at the LHC experiments are compatible with dark matter masses ranging from a few GeV to close to a TeV, as opposed to the requirement of keV-MeV dark matter in simple FIMP scenarios with LLP. In addition, the model presents hitherto unexplored interesting possibilities in the LLP searches, like (i) LLP to LLP to SM cascade decays, which could be searched for within the LHC detectors and (ii) heavy neutral particle decaying within MATHUSLA with two jets and large missing energy. A supplementary aspect of the model is the presence of a heavy neutrino facilitating Type-I seesaw mechanism without disturbing the dark matter side.

Contents

1	Introduction	1
2	Model details	3
3	Freeze-in solution	6
3.1	Two-body decay of χ^+ with $m_\chi > m_S + m_\psi$	7
3.2	Three body decay of χ^+ with $m_\psi + m_N + m_\ell < m_\chi < m_S + m_\psi$	8
4	Exploring freeze-out possibility	13
4.1	Region with large mass splitting: $m_\chi \gg m_\psi$	13
4.2	Region with almost degenerate case: $m_\chi \sim m_\psi$	14
5	Collider signatures	16
5.1	Long-lived charged fermion, χ^+	18
5.2	Long-lived charged scalar, S^+	20
5.3	Long-lived neutral fermion, N	21
6	Conclusion	22
A	Boltzmann Equations	24
B	Constraint from $H \rightarrow \gamma\gamma$	25
C	Constraint from Invisible Higgs decay	25
D	Direct Detection Constraints	26

1 Introduction

The presence of dark matter (DM) constituting about 27% [1] of the energy content of the universe is now established beyond reasonable doubt. The observation of cosmic microwave background radiation with tiny anisotropy as measured precisely by the PLANCK experimental collaboration reveals that cold non-baryonic content of the matter density is $\Omega_{cmb}h^2 = 0.1194 \pm 0022$ [1]. The most studied DM candidates are Weakly Interacting Massive Particles (WIMP), which are thermally produced in the early universe with the relic density surviving after the freeze-out. The attraction of its required annihilation cross section falling in the electroweak ball-park for masses of the order of 100 GeV, therefore providing many natural candidates including the lightest supersymmetric particles [2], are being challenged by the null results of recent direct detection experiments [3–14]. In simple scenarios of WIMP models, the nuclear scattering cross section relevant to the direct detection experiments and the annihilation cross section relevant to the relic density are controlled by the same couplings. This include singlet dark matter scenario (please see Ref. [15] for a recent review), the gauged extensions like the Inert Higgs Doublet/Triplet Model [16–23], fermionic dark matter models having scalar mediated interaction with the SM sector [24–27], and vector

dark matter models [28]. A comprehensive summary of these Higgs portal models is presented in a recent review in Ref. [29].

This push-and-pull between the two experimental measurements has cornered minimal WIMP scenarios. There are many attempts to alleviate this contest by providing mechanisms for the annihilation process, which are irrelevant to the direct detection process. This includes multipartite dark matter models [30–39] with possible conversions from one type to another playing crucial role in achieving the right relic density in specific parameter regions, without affecting the direct detection. The presence of partner particles, having the same symmetry that protects the stability of the dark matter candidate, present in some of these models naturally provides additional annihilation channels which are not relevant to the direct detection. While these attempts are praiseworthy, new directions of thought have emerged providing other equally viable solutions. An attractive possibility is to make the requirement of the annihilation process irrelevant. This is achieved by imagining non-thermal production of the dark matter particles slowly, and gradually building up the required relic density. The mechanism, popularly known as *freeze-in mechanism* [40] as opposed to freeze-out of the WIMP, needs much smaller couplings, thus the particles are called Feebly Interacting Massive Particles (FIMP) [40]. In this case, the direct detection limits are not applicable, as the nuclear scattering cross sections are too small to be probed in the present or near future experiments. However, it may be noticed that the FIMP mechanism works usually with a thermally produced partner particle decaying very slowly to the dark matter particle [41–46]. Such feeble decays make these partner particles live longer than a typical unstable particle. For example, if produced in proton-proton collisions at the LHC, such long-lived particles (LLP) could propagate to perceivable distance before they decay. It provides a possibility for a new way of identifying these scenarios at the collider experiments. Signatures typically include displaced vertex, disappearing charged tracks, and even kinks on the charged tracks. LHC is on the lookout for long-lived particles [47–63]. Apart from the dark matter scenarios discussed above, LLP appears in extra-dimensional models [64, 65], special scenarios in supersymmetry with very narrow mass splitting between the decaying particle and the final state particles [66–71], SM extension with light neutrino mass [72, 73] and models explaining baryogenesis [74, 75]. The high-luminosity version of the LHC (HL-LHC) has dedicated upgrades keeping in view the possible signatures of the LLP [73, 76–78]. In addition, within the LHC complex a dedicated detector known as (MAssive Timing Hodoscope for Ultra Stable neutral pArticles) MATHUSLA [79, 80] is proposed as a large volume surface detector specifically looking for LLP. Detailed study of LLP signatures at the LHC in simplified FIMP models is carried out by [81–83], which shows that mass of the dark matter particles should be in the keV - MeV range to be compatible with dark matter relic density, at the same time providing decay lengths of the partner particles that could be probed by LHC.

In this work, we consider a novel scenario where a fermionic dark matter (ψ) is produced from the slow decay of a charged fermion (χ^+). This necessitates the presence of a charged bosonic degree of freedom, which we consider as a charged scalar S^+ for simplicity, allowing χ^+ to decay through $\chi^+ \rightarrow \psi S^+$. The Yukawa coupling corresponding to this interaction can be adjusted to obtain the required relic abundance of the dark matter. Considered as an $SU(2)_L$ singlet, the charged scalar requires the presence of a gauge singlet neutral fermion N for it to decay via $S^+ \rightarrow N\ell^+$ channel. The Yukawa coupling corresponding to this interaction is independent of the dark sector dynamics. In particular, it is possible that it is small enough to make the charged scalar have sufficiently large decay length to leave distinct LLP signature at the LHC. On the other hand, if the Yukawa coupling in the dark sector is

large enough to accommodate thermal production of the dark matter, we have the WIMP scenario with freeze-out relic density. However, one should be careful in dealing with large Yukawa couplings as, in the absence of tree-level diagrams, they can still contribute to the direct detection cross section through photon/ Z boson mediated penguin diagrams.

Typically, one may imagine that when thermal production is enabled, the non-thermal production through the charged fermion decay is not significant. However, an interesting scenario arises when the non-thermal production adds significantly to the number density along with the thermal production. Such a scenario would emerge when the relevant couplings and masses are in favourable ranges. The relic density, in this case, will be dictated by the thermal freeze-out mechanism. Nevertheless, this possibility will lead to more viable regions of parameter space, with consequent effects in other sectors including the collider processes. The result of all these effects provide a feasible mechanism of dark matter of mass in a wide range of a few GeV to close to a TeV, along with LLP that could be probed through the LHC experiments. Presence of multiple LLPs potentially provide another interesting aspect to their search at the LHC through cascade decay of $LLP \rightarrow LLP \rightarrow SM$, adding a different dimension to the LLP searches. In this article, we shall study the details of the dark matter scenario of the model and indicate the collider possibilities, with the detailed collider phenomenology deferred to a future publication.

We organise this paper with the details of the model given in Section 2, followed by the numerical analysis and discussion of results related to the freeze-in scenario presented in Section 3, and freeze-out scenario presented in Section 4. In Section 5 we take a brief look at the collider signatures of the LLP associated with this study, and finally, conclude in Section 6.

2 Model details

We consider dark matter to be a gauge singlet fermion denoted by ψ , which is made stable by imposing a Z_2 symmetry under which it is odd. The non-thermal production of ψ is realised through the slow decay of a partner charged fermion χ^+ , which is a vector-like gauge singlet. χ^+ and ψ have the same transformation property under the Z_2 . This decay necessitates the presence of a charged gauge singlet scalar field, denoted here by S^+ , which in turn decays to the charged standard lepton and newly introduced gauge singlet vector-like neutral fermion, N . The Yukawa interaction of N with the Standard Model (SM) Higgs field and the left-handed lepton doublet along with its explicit Dirac mass term, could be made use of to generate the neutrino mass through type-I seesaw mechanism. Keeping this in mind, we introduce three copies of N in our set up. The additional particle spectrum along with their hypercharge and Z_2 charge are given in Table 1. All the SM fields are even under the Z_2 .

field	Y	Z_2
S^+	+2	+
N_1, N_2, N_3	0	+
χ^+	+2	−
ψ	0	−

Table 1: Additional fields and their charges.

With the above particle content, the Lagrangian of the model is given by

$$\begin{aligned}
\mathcal{L} = & \mathcal{L}_{SM} + (D_\mu S)^\dagger (D^\mu S) + \bar{\chi} i \gamma^\mu D_\mu \chi + \bar{\psi} i \gamma^\mu \partial_\mu \psi + \sum_i \bar{N}_i i \gamma^\mu \partial_\mu N_i \\
& - m_\chi \bar{\chi} \chi - m_\psi \bar{\psi} \psi - \sum_i m_{N_i} \bar{N}_i N_i \\
& - \left(y_1 \bar{\chi} S \psi + \sum_i y_{2i} \bar{N}_i S \ell_i + \sum_i y_{N_i} \bar{L}_i \tilde{\Phi} N_i + h.c. \right) \\
& - (\mu_S^2 S^\dagger S + \lambda (S^\dagger S)^2 + \lambda_1 S^\dagger S \Phi^\dagger \Phi)
\end{aligned} \tag{2.1}$$

where Φ represents the SM Higgs doublet, L_i and ℓ_i denote the SM left-handed lepton doublet and right-handed charged lepton singlet, respectively. The summation index i runs from 1 to 3 indicating the three flavors of leptons. The Yukawa couplings and the mass parameter m_{N_i} are taken to be diagonal, so that the interactions do not lead to any flavor-violating processes. However, the contribution to $g - 2$ of the charged leptons arising at the one-loop level are proportional to y_{2i}^2 , and therefore require to be small [84, 85] for the first two generations, while the $i = 3$ it could be more relaxed. Moreover, the presence of neutral fermions N_i can explain neutrino mass generated via Type-I seesaw mechanism. The mass matrix in the interaction basis is

$$\begin{pmatrix} 0 & v Y_N \\ v Y_N^T & m_N \end{pmatrix}, \tag{2.2}$$

where Y_N and m_N are 3×3 matrices with $Y_N = \text{diag}(y_{N_1}, y_{N_2}, y_{N_3})$ and $m_N = \text{diag}(m_{N_1}, m_{N_2}, m_{N_3})$. Keeping m_{N_i} at the GeV-TeV scale requires $y_{N_i} \sim 10^{-8}$ to get the right neutrino mass (of ~ 0.1 eV). The other Yukawa coupling is limited by perturbativity, and thus we consider $y_1 \leq \sqrt{4\pi}$. Electroweak symmetry breaking is controlled purely by the Higgs mechanism involving the Φ field. After the symmetry breaking, the mass of the charged scalar is given by

$$m_S^2 = \mu_S^2 + \frac{\lambda_1 v^2}{2}, \tag{2.3}$$

whereas m_χ and m_ψ are free parameters. In addition to the constraints discussed above, further constraints come from the collider experiments. If kinematically allowed, $\chi^+ \chi^-$ and $S^+ S^-$ pairs could be produced in $e^+ e^-$ collision, leading to dilepton final state accompanied by missing energy. Consequently, to avoid LEP constraints we consider $m_\chi \geq 45$ GeV. Similarly, the Higgs bosons can decay to $S^+ S^-$ pair owing to the quartic coupling, λ_1 , contributing to the Higgs decay. For simplicity, we consider $m_S \geq 63.5$ GeV to kinematically prohibit this decay. On the other hand, possible contributions to $H \rightarrow \gamma\gamma$ and to $H \rightarrow \psi\psi$ through the presence of S^+ and χ^+ in the loop may need attention. We discuss the contribution to the di-photon decay channel in Appendix B. With $m_S = 150$ GeV, this contribution (Eq. B.7) leads to less than 3% contribution for $\lambda_1 = 0.01$. Contribution to the invisible Higgs decay is negligible compared to the standard contributions, as discussed in Appendix C.

Coming to other constraints, the decay pattern of $S \rightarrow N \ell$ could look very similar to supersymmetric slepton decays to neutralinos and leptons, and therefore it is tempting to imagine that the collider constraints from slepton search is applicable to S^+ . However, the SUSY searches are quite model dependent, and thus not applicable as such in our case. For example, constraints on long-lived stau quoted in Ref. [86] is derived within the restricted mass-splitting scenario and within the context of gauge mediated SUSY breaking. Since we have the freedom to choose the couplings and masses within a much larger range, to start

with, we do not consider any such collider constraints. However, in the full considerations of collider phenomenology, these constraints should be included.

Turning to the dark matter side, we have different possibilities arising here depending on the kinematics and couplings. First of all, the dominant mechanism for production of the dark matter ψ is the decay of thermally produced charged fermionic partner, χ^+ . This immediately requires $m_\chi > m_\psi$. The decay proceeds through their coupling with the singlet charged scalar, S^+ . Here, there are two possibilities: (i) when kinematically allowed with $m_\chi \geq m_\psi + m_S$, the decay essentially goes through the on-shell S^+ ($\chi^+ \rightarrow \psi S^+$); (ii) when $m_\psi + m_N \leq m_\chi < m_\psi + m_S$, it results in a three body decay of $\chi^+ \rightarrow \psi S^* \rightarrow \psi N \ell^+$. In the first case, the decay is dictated by a single coupling y_1 , whereas in the second case it is the product of $y_1 y_2$ that matters. As noted above, y_2 is restricted to be small for the first two generations, while it can be more relaxed for the third generation which couples the τ lepton with S^+ . Direct detection experiments can constrain the coupling y_1 through processes at one-loop level. We have discussed the contribution in the Appendix D. To have $\sigma_{\text{SI}}^{\psi\chi} \leq 10^{-46} \text{ cm}^2$ as required by the direct detection experiments, for masses of the order of 100 GeV, the coupling typically comes around $y_1 \lesssim 0.05$.

The strength of all these interactions will dictate the relic density of ψ , the dark matter candidate. In Table 2 we have listed the distinct possibilities that could arise.

Case 1: $m_\chi > m_S + m_\psi$

Mechanism	y_1	m_ψ	Possibilities	Viable?
Thermal production	large	$< m_S$	over-abundance	No
		$> m_S$	$\psi\psi \rightarrow S^+ S^-$ enabled freeze-out	Yes
production through decay of χ^+	small	–	freeze-in to saturation	Yes

Case 2: $m_\psi + m_N < m_\chi < m_S + m_\psi$

Mechanism	$y_1 y_2$	y_1	m_ψ	Possibilities	Viable?
Thermal production	large	any	$< m_S$	over-abundance	No
		restricted	$> m_S$	$\psi\psi \rightarrow S^+ S^-$ is enabled	Yes
Thermal production + production through decay of χ^+	small	small	any	freeze-in to saturation	Yes
		restricted	$> m_S$	$\psi\psi \rightarrow S^+ S^-$ enabled freeze-out	Yes
			$< m_S$	over-abundance	No

Table 2: Distinct scenarios and their viabilities considering relic density of the dark matter.

In the first case with 2-body decay of χ^+ , the coupling y_2 does not affect the scenario. For large values of y_1 , the dark matter ψ is thermally produced. In addition to the decay of χ^+ , the scattering process $S^+ S^- \leftrightarrow \chi^+ \chi^-$ will also be relevant here. The only way to get the right relic density is by taming the dark matter density through its annihilation. This could be achieved in the present model through the pair annihilation of ψ into $S^+ S^-$ pairs and possible co-annihilations, when kinematically allowed. Note that it is the same coupling which dictates the annihilation process as well. On the other hand, for very small y_1 , the slow production of ψ gradually builds up the dark matter density. Apart from y_1 ,

the mass splittings would also play crucial role in getting the right relic density. Moving to the case of 3-body decay of χ^+ as listed in Table 2 Case 2, it is the product of the couplings $y_1 y_2$ which is now relevant. Again, for large values of this coupling combination, ψ is thermally produced, and the over-abundance could be tamed with the pair annihilation of ψ for favourable kinematic ($m_\psi > m_S$) and dynamic ($y_1 > 0.1$, as shown through numerical studies discussed later) conditions. This is quite similar to the large coupling scenario of case 1. On the other hand, for very small values of $y_1 y_2$, there are two different situations. One is that y_1 is also very small. In that case the only relevant mechanism is the freeze-in mechanism. On the other hand, with large enough y_1 thermal production can lead to over abundance when $m_\psi < m_S$, which is tamed through the annihilation process, $\psi\psi \rightarrow SS$ for $m_\psi > m_S$. In this scenario, when $y_1 y_2$ is not too small, significant contribution from non-thermal (decay of χ) production of ψ can add to the relic density. However, a proper treatment of this requires solving the coupled Boltzmann equation for both ψ and S , as ψ and S may no more be in chemical equilibrium. In the present discussion, we shall restrict ourselves to the two limiting cases of either the thermal production or non-thermal production dominate, with the other contribution negligible.

In the following sections we shall discuss the freeze-in and freeze-out scenarios separately, and present a numerical study to understand the specific situations and viable parameter space regions in each of these cases.

3 Freeze-in solution

The production of DM candidate ψ through the slow decay of gauge produced χ^+ gives rise to the freeze-in mechanism by building the DM density to the required value. The decay of χ^+ is controlled by the Yukawa coupling y_1 with S^+ and ψ . When kinematically possible, it will be a two body decay with S^+ produced on-shell. On the other hand, if $m_S + m_\psi \geq m_\chi$, it is a three body decay to final state $\psi N \ell$, mediated by a virtual S^+ . In the latter case, the decay is dictated by the Yukawa coupling y_2 of $S^+ N \ell^+$ along with y_1 . While in the first case y_1 is required to be small enough for freeze-in to be possible, in the second case the product $y_2 y_1$ should be of this order. The relic density depends on the decay width, Γ_{χ^+} and the masses of the parent particle and the DM candidate through the relation [40]

$$\Omega_\psi h^2 = \frac{2.19 \times 10^{27} g_\chi}{g_*^S \sqrt{g_*^\rho}} \frac{m_\psi \Gamma_{\chi^+}}{m_\chi^2}, \quad (3.1)$$

where $g_*^{S,\rho}$ are effective degrees of freedom in the bath at freeze-in temperature $T \sim m_\chi$. g_χ denotes the number of degrees of freedom corresponding to the decaying particle χ^+ , which is equal to 2 for a fermion.

We shall consider these two distinct cases separately in our numerical analysis below. The charged scalar decays to $N \ell^+$, enabled by the Yukawa coupling y_{2i} . In the first case of two body decay of χ^+ , the decay of S^+ is decoupled from the freeze-in mechanism, and therefore y_2 can be independently varied. As mentioned in the introduction, this coupling can potentially induce anomalous $g - 2$ for the charged SM leptons, and therefore y_2 is required to be small. With small y_2 , it is possible that S^+ has delayed decay, but within the detectors of the LHC experiments. The heavy neutrino N can decay through its coupling with the SM neutrino and the Higgs boson, y_N , which is required to be very small to generate the right neutrino mass. Thus, potentially, N could also be long-lived, and mostly decay outside the detector complex giving missing energy signature. In the second case of the three-body decay of χ^+ ,

although not decoupled from the relic density formation, y_2 can be such that S^+ has delayed decay to leave distinct signature at the collider detectors. We shall discuss the signatures of this long-lived S^+ in the later section. Below we shall focus on the dark matter side of the model and find viable parameter space regions compatible with observations. Feynman diagrams corresponding to the decay of χ^+ in the two cases, and that of the S^+ decay are given in Fig. 1a, 1b and Fig. 1c, respectively. We shall discuss these two cases separately below.

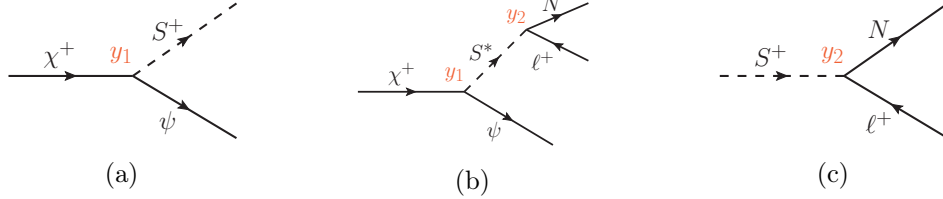


Figure 1: Feynman diagram showing the two body (a) and three body (b) decays of χ^+ , and the Feynman diagram showing the decay of S^+ (c).

3.1 Two-body decay of χ^+ with $m_\chi > m_S + m_\psi$

In this case, the DM candidate is produced through the two-body decay of the χ^+ which is gauge produced abundantly, and in thermal equilibrium. The decay width of χ^+ is given in this case by,

$$\Gamma_{\chi^+ \rightarrow S^+ \psi} = \frac{y_1^2}{16\pi m_\chi^3} \left[(m_\chi + m_\psi)^2 - m_S^2 \right] \left[(m_\chi^2 - m_S^2 - m_\psi^2)^2 - 4m_S^2 m_\psi^2 \right]^{\frac{1}{2}} \quad (3.2)$$

One may notice that, in principle, a pair of ψ can annihilate into $S^+ S^-$ pairs when kinematically feasible. Such a reaction will be a t -channel process mediated by χ^+ as shown in the Feynman diagram in Fig. 2a. In addition to the pair annihilation, when the mass splitting is favourable, the co-annihilation processes with Feynman diagrams shown in Fig. 2b, 2c, 2d could also affect the number density of the dark matter. However, the cross section of the pair annihilation process is proportional to y_1^4 , while that of all other processes are proportional to y_1^2 , the same coupling that controls the slow production leading to freeze-in mechanism. Thus, the annihilation cross sections are expected to be negligibly small leaving no signature in the relic density.

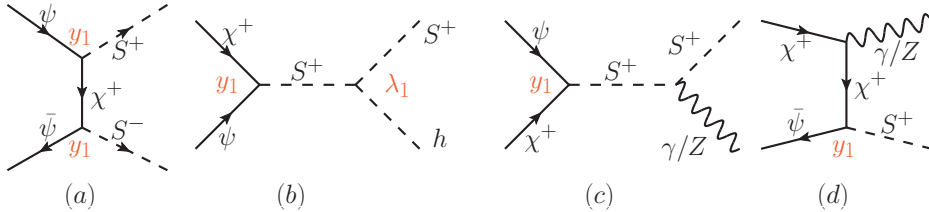


Figure 2: Pair annihilation (a) and co-annihilation channels (b, c, d) of the dark matter ψ .

The relic density for a wide range of parameters is computed using MATHEMATICA with the help of the above relation and compared with the value allowed by PLANCK [1] experiment. The relic density in this case depends on the single Yukawa coupling y_1 , and the

masses of the participating particles, m_χ , m_S and the dark matter particle m_ψ . We fix the other parameters, which do not affect the relic density as $\lambda = \lambda_1 = 0.01$, $y_N = 10^{-8}$, $y_2 = 10^{-9}$.

All the three copies of the neutral vector fermion mass are fixed at $m_N = 30$ GeV in our scan. While the decay width of S^+ has a kinematic dependence on m_N , the width of χ^+ itself is not affected by this parameter. The range of the relevant parameters used in the scan are given in Table 3. All through we have maintained the mass splitting so that χ^+ can undergo a two body decay. Scanning over 50,00 random points, we selected those satisfying the right relic density, and analysed those for possible correlations and constraints.

$1 \text{ GeV} \leq m_\psi \leq 1000 \text{ GeV}$	$65 \text{ GeV} \leq m_S \leq 1000 \text{ GeV}$
$m_S + m_\psi \leq m_\chi \leq 1 \text{ TeV}$	$10^{-14} \leq y_1 \leq 10^{-8}$

Table 3: Range of relevant parameters considered for the numerical scan in this study.

In Fig. 3 the correlation between y_1 and relevant masses are given. As seen from y_1 vs. m_S larger masses require larger couplings to compensate for the effect of the phase space. On the other hand, in the case of y_1 vs. m_ψ , the phase space suppression for larger m_ψ is smaller compared to the enhancement in the invariant amplitude, as is clear from the decay width expression in Eq. 3.2. Further, there is an additional factor of m_ψ in the expression for $\Omega_\psi h^2$ in Eq. 3.1, pulling down the decay width to maintain the same relic density. The correlation between the parent particle mass (m_χ) and y_1 clearly indicates that y_1 is preferred to be in the range of $10^{-13} - 10^{-9}$ to satisfy the required relic density. As expected, smaller mass splitting $\Delta m_{\chi S} = m_\chi - m_S$ requires larger y_1 to compensate for the narrow phase space available. The right-bottom plot in Fig. 3 shows y_1 against m_S for two different m_χ values of 300 GeV and 1 TeV. The mass splitting $\Delta m_{S\psi} = m_\psi - m_S$ is indicated in different colours. While in the case of lighter m_χ the mass splitting is not very relevant, in the case of heavier χ^+ smaller y_1 is preferred for larger m_ψ values, in agreement with top-right plot and the discussion above.

3.2 Three body decay of χ^+ with $m_\psi + m_N + m_\ell < m_\chi < m_S + m_\psi$

In this case, the decay of χ^+ to on-shell S^+ is not kinematically possible. However, three body decay enabled through a virtual S^+ decaying into $N\ell$ pair, as illustrated in the Feynman diagram in Fig. 1 (b), produces the dark matter. The decay width $\Gamma_{\chi^+ \rightarrow \psi N \ell^+}$ is proportional to $(y_1 y_2)^2$, as given by

$$\Gamma_{\chi^+ \rightarrow \psi N \ell^+} = \frac{(y_1 y_2)^2}{256 \pi^3 m_\chi^3} \int_{X_{\min}}^{X_{\max}} dX [(m_\chi^2 - X - m_\psi^2)^2 - 4X m_\psi^2]^{\frac{1}{2}} [(X - m_N^2 + m_\ell^2)^2 - 4X m_\ell^2]^{\frac{1}{2}} \times \frac{[(m_\chi + m_\psi)^2 - X] [X - m_N^2 - m_\ell^2]}{X [(X - m_S^2)^2 + \Gamma_S^2 m_S^2]}, \quad (3.3)$$

where $X_{\max} = (m_\chi - m_\psi)^2$ and $X_{\min} = (m_N + m_\ell)^2$. Having the product of the couplings controlling the production, unlike in the previous case, the following distinct possibilities arise in this case, depending on the mass splitting $\Delta m_{\psi S} = m_\psi - m_S$.

1. $y_1 y_2 \ll 1$, $y_1 \ll 1$ for any $\Delta m_{\psi S}$: In this case, the coupling y_1 being small ($\leq 10^{-8}$), the annihilation channel $\psi\psi \rightarrow S^+ S^-$ is not effective leading to a situation similar to

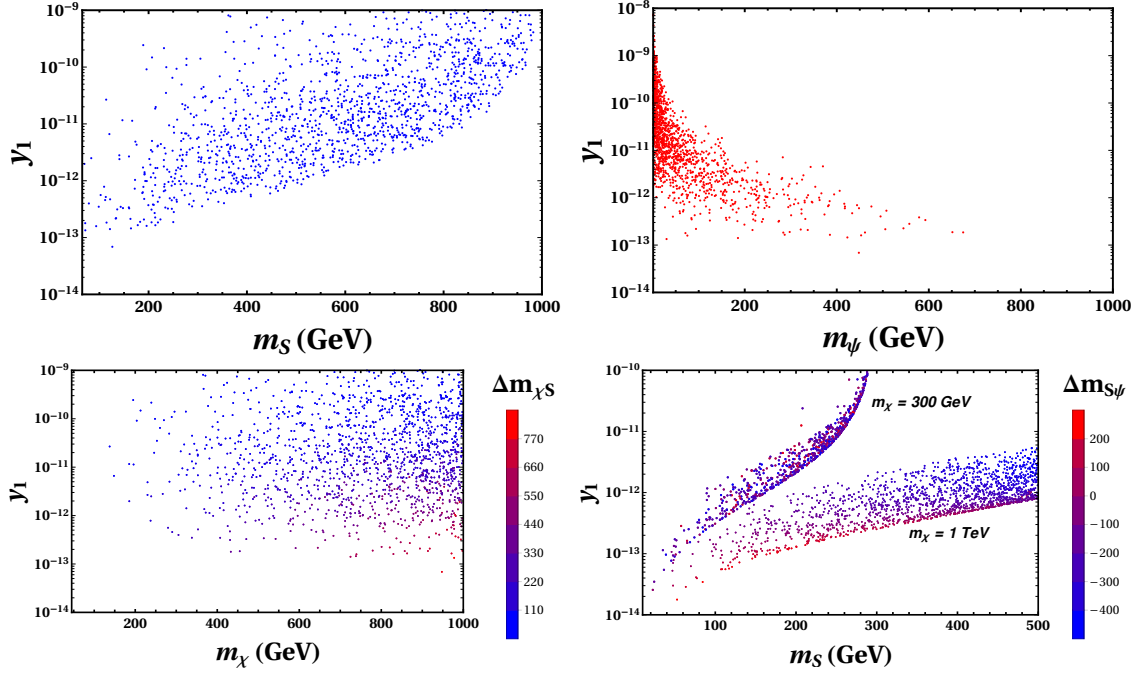


Figure 3: Yukawa coupling y_1 vs. mass of the non-SM particles that satisfy the relic density bound. In plots in the top row and bottom-left m_S , m_ψ and m_χ are varied from a few GeV to 1 TeV. Other parameters are as per Table 3. In the bottom-right plot, $m_\chi = 300$ GeV and 1 TeV are considered, while m_ψ is varied in the full range.

Case 1 described in Section 3.1. ψ produced via 3-body decay of $\chi^+ \rightarrow \psi N \ell^+$ slowly saturates to leave the required relic density. We shall show that, for a large range of mass of S^+ , it is possible to find couplings compatible with the freeze-in scenario in the range of $10^{-11} \leq (y_1 y_2) \leq 10^{-5}$.

2. $y_1 y_2 \ll 1$, $y_1 \sim 1$, with $\Delta m_{\psi S} < 0$: In this case the production is mostly thermal through $SS \rightarrow \psi\psi$ with possible addition from the decay of χ^+ , the contribution being dependent of the value of $y_1 y_2$. Since the annihilation $\psi\psi \rightarrow S^+ S^-$ is kinematically disfavoured, it results in over-abundance. The co-annihilation channels could, however, be relevant, as the kinematics may not restrict those.
3. $y_1 y_2 \ll 1$, $10^{-8} < y_1 \sim 1$, with $\Delta m_{\psi S} > 0$: In this case again, the thermal production through $SS \rightarrow \psi\psi$ and from the decay of χ^+ builds up the number density of the dark matter particle. However, owing to sizeable y_1 the now kinematically allowed annihilation cross section is significant, leading to favourable relic density through freeze-out. The resultant relic density at the saturation depends on various factors including the rate of decay of χ^+ and the annihilation cross section of $\psi\psi \rightarrow S^+ S^-$ channel.

We shall not discuss case 2 above any further, as this does not lead to the right relic density. The other two cases, case 1 where the thermal production and annihilation are not relevant, owing to small value of y_1 , and case 3 with large y_1 are discussed with numerical results below.

In the absence of annihilation: We shall first consider the situations 1 listed above, where the annihilation does not play a role. Scanning the parameters within the range specified by Table 4, we explore the parameter space providing the right relic density.

$1 \text{ GeV} \leq m_\psi \leq 1000 \text{ GeV}$	$65 \text{ GeV} \leq m_S \leq 1000 \text{ GeV}$
$m_N + m_\psi \leq m_\chi \leq 1 \text{ TeV}$	$10^{-12} \leq y_1 y_2 \leq 10^{-5}$

Table 4: Range of relevant parameters considered for scan. The condition, $m_\chi < m_\psi + m_S$ to kinematically disable $\chi^+ \rightarrow S^+ \psi$ with S^+ on-shell is further imposed. A few selected m_N values are considered for the analysis.

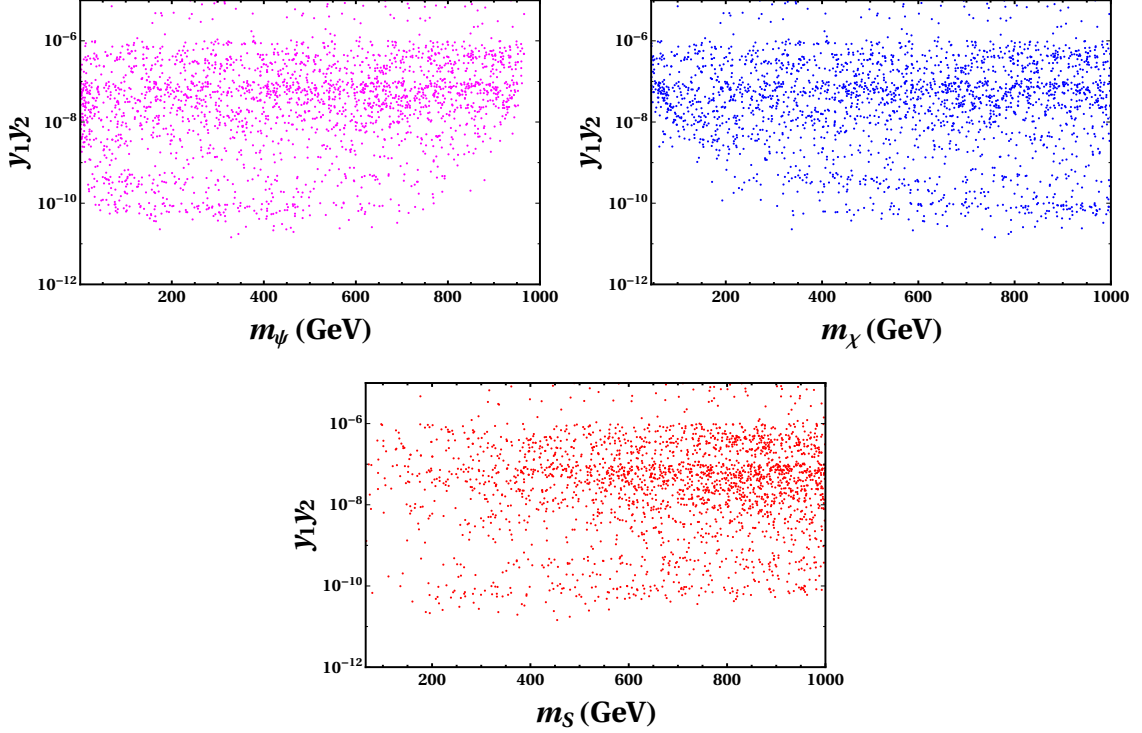


Figure 4: Correlation between the relevant coupling and the dark matter mass m_ψ (left), the decaying parent particle mass m_χ (right) and the associated charged scalar S^+ (bottom), satisfying the relic density bound.

In Fig. 4 the coupling combination $y_1 y_2$ is plotted against m_ψ (top left figure), m_χ (top right figure) and m_S (bottom figure). Generically, the product of the coupling below 10^{-10} is not possible, with a few points between 10^{-11} and 10^{-10} corresponding to relatively heavier χ^+ and lighter m_S so that the propagator factor compensates for the small coupling. For lighter χ^+ below 200 GeV, the coupling is mostly larger than 5×10^{-10} , which is filtered down to slightly lower than 10^{-10} for masses between 200 and 400 GeV, above which it is possible to go down by one more order. The correlation between m_χ and m_ψ is plotted in Fig. 5, where the effect of m_N is indicated with two illustrative values of $m_N = 30$ and 200 GeV. The effect mostly arises from the kinematic limit constraint of $m_\chi > m_\psi + m_N$. In the right-hand-side plot in Fig. 5, the effect of the coupling on this correlation is indicated for three different choices of couplings, for a fixed $m_N = 30$ GeV. Note that the decay width depends on the inverse powers of its mass, and therefore, require larger values of the couplings for heavier χ^+ , as clearly indicated in the three cases presented in the plot.

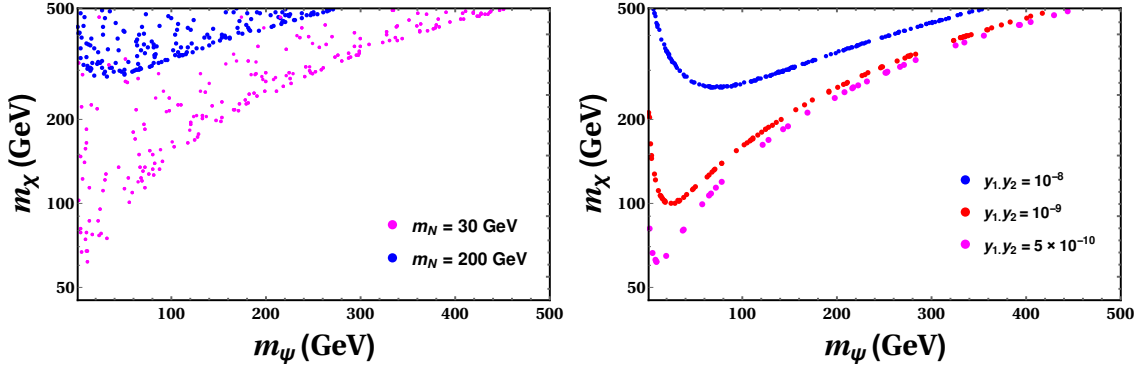


Figure 5: Correlation between m_ψ and m_χ in the case of freeze-in with 3-body decay of χ^+ . The *left* plot allows m_S and $y_1 y_2$ to vary within the specified range, while the *right* plot has $m_S = 800$ GeV and three different indicative $y_1 y_2$ values. m_N is fixed at 30 GeV in the *right* plot.

In the presence of annihilation: The third situation listed above, which includes the effect of sizable annihilation cross sections is interesting, however not usually considered in the literature. In most situations studied, a single coupling parametrised the interactions. Freeze-in mechanism requiring this to be small naturally makes the effects of annihilation irrelevant. However, as we demonstrate here, in the presence of an additional coupling such as present in the scenario discussed in this article provides a natural framework where along with the thermal production, significant amount of DM is produced through the decay of the associated particle. In presence of annihilation, this leads to an interesting interplay of the thermal and non-thermal production of ψ . When y_1 and $y_1 y_2$ both are small, ψ is not in equilibrium with the thermal bath and is only produced from the decay of χ . However, S^+ , being Gauge produced, if y_1 increases, $\psi\psi \rightarrow SS$ forward and backward scatterings also produce ψ from the thermal bath and slowly drive it towards equilibrium in the early Universe. This feature is illustrated in Fig. 6, where the yield of ψ is plotted against m_ψ for a fixed $y_1 y_2$ but for different y_1 values. The green curve can be considered as the typical non-thermal production via freeze-in due to the minuscule $\langle\sigma v\rangle$ (corresponding to $y_1 \sim 10^{-8}$). The blue and the red line correspond to larger y_1 which clearly show the increasing effect of the thermal production of ψ from the bath in the early Universe. However, for such values of $\langle\sigma v\rangle$, the non-thermal decay is still the dominant production channel and we see the effect of saturation of yield when it becomes Boltzmann suppressed, similar to the freeze-in scenario. Now, on increasing y_1 further, the thermal production becomes more dominant and the typical freeze-out scenario is recovered, which can be seen from the brown, pink, magenta and the black line. Similar to the WIMP freeze-out, these cases give overabundance or underabundance depending on the $\langle\sigma v\rangle$ value considered.

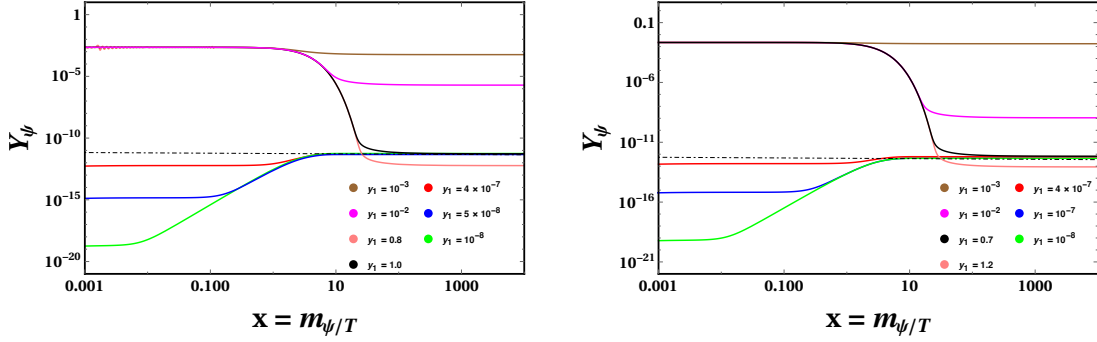


Figure 6: Plots showing interplay of the thermal and non-thermal production of ψ for various values of y_1 . The non-thermal production of ψ from χ decay is kept fixed with $y_1 y_2 = 10^{-10}$ (left) and $y_1 y_2 = 10^{-6}$ (right). The dot-dashed lines represent the correct relic density for the specific benchmark point $m_S=50$ GeV, $m_\psi=80$ GeV, $m_\chi=120$ GeV in the left plot and $m_S=463$ GeV, $m_\psi=941$ GeV, $m_\chi=972$ GeV in the right plot. m_N is fixed at 30 GeV.

A few benchmark points compatible with this scenario are presented in Table 5¹, indicating the cases when pair annihilation and co-annihilation channels contribute significantly. For clarity, we have included the respective cases with small y_1 , where the effect of annihilation is absent, and the correct relic density is not achievable. While the results are presented for a fixed $m_N = 30$ GeV, we have checked that it produces the relic density within the same order of magnitude for a range of m_N from 1 GeV to a couple of 100 GeV. It is clear from Fig. 6 that based on the couplings, the DM is either following freeze-in saturation or is driven towards thermal freezeout. This is largely due to the coupling y_1 which, for large values, is responsible for sufficient energy exchange between S^+ and ψ in the early Universe, therefore, suppressing the non-thermal production of ψ . If the production and annihilation channels of ψ could be considered independently, then it would be possible to restrict its production to only non-thermal decay of χ and annihilate through some other coupling which does not contribute to the energy exchange of DM with thermal bath. A possible way-out is to consider cases like mediator driven annihilation and conversion as the possible modes of annihilation of ψ . It is well known that for very small mass splitting between ψ and χ , $\chi\chi \rightarrow \text{SM SM}$ processes contribute substantially to the relic density of ψ . In this model, these processes are Gauge mediated, hence independent of y_1 . Hence, even if we take both y_1 and y_2 small enough to ensure only non-thermal decay of χ^+ , the production and the annihilation of ψ still remains independent of each other. Ref. [87] discusses a similar situation and on solving out-of-equilibrium Boltzmann eqns. (see Eqn. 9 and 10 of Ref. [87]) for DM candidate and the mediator, an interesting situation is obtained which can be interpreted as an intermediate stage between freeze-in and freeze-out scenario, where the non-thermal over production can be tamed by sufficient annihilation. However, as seen from the parameter choice of this plot, this is valid only for a small mass splitting between the DM candidate and the mediator, which is not of much importance for our discussion since the viable parameter space is very

¹In Fig. 6 and Table. 5, large values of y_1 is taken to show the effect of the interplay between the thermal and non-thermal production of ψ . However, direct detection diagrams in one loop constrains this coupling to $y_1 \lesssim 0.05$. This implies that this coupling in the allowed limit is not sufficient to satisfy the observed relic density, but it can make the thermal production dominant over the non-thermal case and lead to overabundance. We will show later on in the discussion of freezeout that coannihilation and mediator annihilation channels can satisfy the observed relic even with small y_1 .

m_χ	m_ψ	m_S	$y_1 y_2$	y_1	Ωh^2
515.5	485.4	176.3	4.7×10^{-6}	10^{-8}	0.119
				10^{-2}	2.1×10^5
				0.5	0.12
				1.0	0.008
394.5	352.9	338.5	1.1×10^{-8}	10^{-8}	0.119
				10^{-2}	2.2×10^6
				0.98	0.12
				1.5	0.02
460.6	300.2	214.1	3.72×10^{-11}	10^{-8}	0.119
				10^{-2}	5.9×10^5
				0.67	0.12
				1.0	0.02

Table 5: Benchmark points showing the effect of the additional thermal production of ψ with normal non-thermal production from χ^+ decay. For negligible y_1 , the correct relic density is achieved by non-thermal production only. Increasing y_1 enhances the thermal production of ψ through $SS \leftrightarrow \psi\psi$ channel in the early Universe, suppressing the non-thermal production. Therefore, the freeze-out scenario is recovered, where overabundance or underabundance is dictated by the choice of y_1 . All masses are in GeV. The mass of the neutral fermion is set to $m_N = 30$ GeV in all cases.

much contrived.

4 Exploring freeze-out possibility

The model can also explain thermal dark matter, such as the standard WIMP scenario through thermal freeze-out, which is viable over a large regions of parameter space. In this case, it is assumed that the DM candidate ψ is already in equilibrium with the thermal bath. Hence we no longer require the DM interaction coupling y_1 to be very small unlike freeze-in scenario, therefore it is considered to be of the order of unity. All the possible annihilation diagrams are given in Fig. 2. Based on the mass splitting between the dark sector particles (χ^+ and ψ), the relic density will be dominated by either annihilation of DM into SM particles (Region 1) or co-annihilation between the dark fermions (Region 2). Fig. 2(a) represents the only diagram possible when ψ pair annihilates into S^+S^- pairs through t -channel mediation of χ^+ . Fig. 2(b)-(d) represent the co-annihilation channels which become effective only when the mass splitting between incoming particles is very small. The model is implemented in Feynrules [88] and the freeze-out relic density computation is done using micrOMEGAs [89].

The parameter space is classified into two regions of $m_\chi \gg m_\psi$ and $m_\chi \sim m_\psi$, with the co-annihilation channels becoming important in the latter case. We shall discuss these two regions separately in the following subsections.

4.1 Region with large mass splitting: $m_\chi \gg m_\psi$

The only pair annihilation of the dark matter in this region proceeds through the t -channel to a final state of S^+S^- pairs shown in Fig. 2(a), with the cross section proportional to y_1^4 . The co-annihilation process have negligible contribution as the cross section for such process goes like the exponential of mass splitting between the dark matter and the partner, $e^{-(m_\chi - m_\psi)/m_\psi}$ [90]. To study the relic compatible parameter space regions, we scan over the

available/relevant range of parameters and compute the relic density using micrOMEGAs. As in the earlier case, the irrelevant quartic couplings, λ and λ_1 are fixed at 0.01, and the Yukawa coupling dictating the neutrino mass are set at $y_{N_i} \approx 10^{-8}$. The mass of the neutral fermions are set to $m_N = 30$ GeV, while the Yukawa coupling between $S^+ N \ell$ is taken as $y_2 = 10^{-6}$. The parameters, which are relevant to the annihilation process here are varied randomly in the range given in Table 6.

$1 \text{ GeV} \leq m_\psi \leq 1 \text{ TeV}$	$m_\chi = m_\psi + (100, 800) \text{ GeV}$
$65 \text{ GeV} \leq m_S \leq 1 \text{ TeV}$	$0.0 \leq y_1 \leq 3.0$

Table 6: Range of parameters considered for the scan in Region 1: $m_\chi \gg m_\psi$ with thermal freeze-out of dark matter ψ .

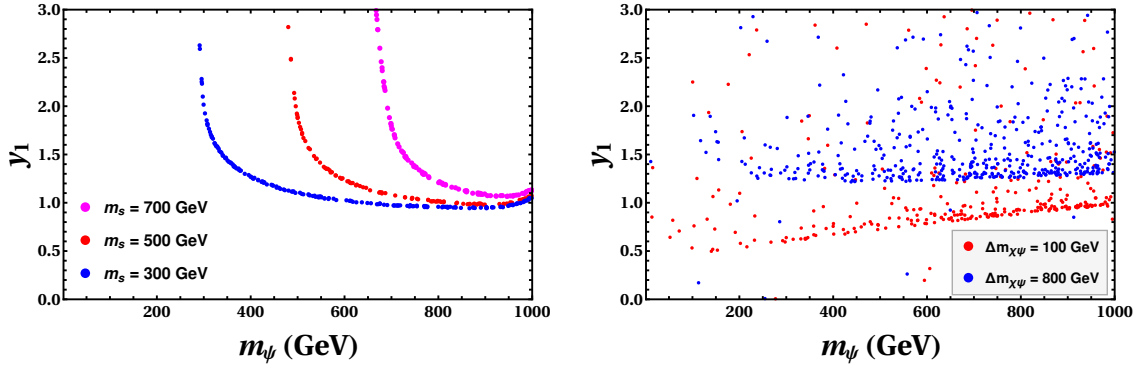


Figure 7: y_1 vs. m_ψ for specific values of m_S in agreement with the measured DM relic density; Left: for a fixed propagator mass of $m_\chi = 1$ TeV; Right: for varying m_χ with the mass splitting fixed at $m_\chi - m_\psi = 100$ GeV (red) and 800 GeV (blue) keeping $65 \leq m_S \leq 1000$ GeV.

In Fig. 7, the variation of the coupling y_1 is plotted against the DM mass. The $\psi\psi \rightarrow S^+ S^-$ annihilation channel opens up at different S^+ values, as shown in the left plot in Fig. 7, for a fixed χ^+ mass of 1 TeV. In the right plot of Fig. 7, m_χ is varied for the entire range of m_ψ keeping the mass splitting fixed at two specific values. For smaller mass splitting, a relatively lighter propagator reduces the demand on the requirement of large coupling. However, to be compatible with the direct detection limits of $y_1 \leq 0.05$, highly degenerate region of the parameter space may be required, as explained towards the end of the next subsection. It is to be noted here that if S^+ was not charged, the one loop penguin diagrams (Fig. 14) contributing to direct search would not contribute, but still the strength of the new physics coupling would determine the interplay between the nonthermal and thermal production, even leading to freezeout for a wider parameter space. Because of this generic feature, we have kept the full range of y_1 in the analysis, although for our particular case freezeout is restricted to a narrow window of the parameter space.

4.2 Region with almost degenerate case: $m_\chi \sim m_\psi$

In this region, as the mass difference between χ^+ and ψ is very small, the effect of the co-annihilation channels become important. Unlike Fig. 2(a), these channels provide correct relic

density even when $m_\psi \leq m_S$. This is because ψ can now annihilate into S^+ and a photon or a Z boson provided $2m_\psi \geq m_S/(m_S + m_Z)$ (Fig. 2(c),(d)). Setting a non-zero value of λ_1 enables the process considered in the diagram in Fig. 2(b), although the effect of this cross section is very small. However, since λ_1 is fixed at a small value ($= 0.01$) in the analysis, this contribution is always negligible. We consider the ranges of parameters given in Table 7 while performing the scan.

$1 \text{ GeV} \leq m_\psi \leq 1 \text{ TeV}$	$m_\chi = m_\psi + 1, 5, 10 \text{ GeV}$
$65 \text{ GeV} \leq m_S \leq 1 \text{ TeV}$	$0.0 \leq y_1 \leq 3.0$

Table 7: Range of parameters considered for the scan in Region 2: $m_\chi \sim m_\psi$ with thermal freeze-out of dark matter ψ .

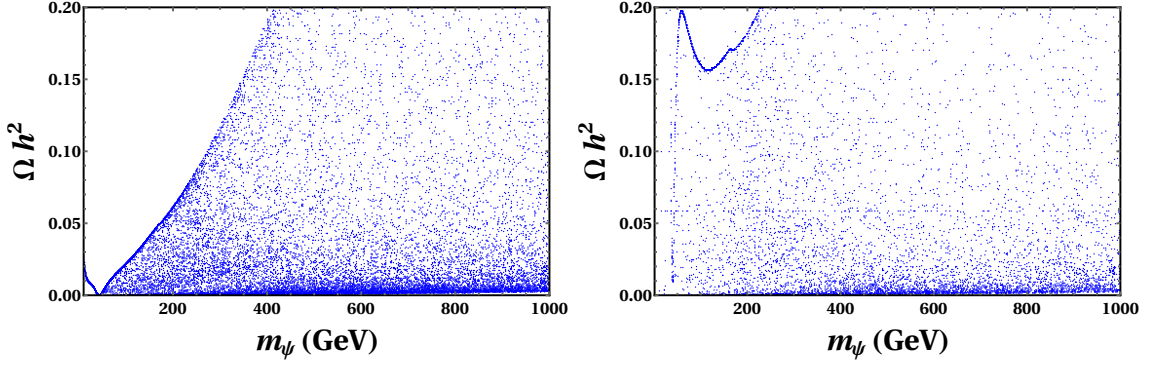


Figure 8: DM relic density vs. DM mass for mass splitting between dark sector particles fixed at 1 GeV (left) and 5 GeV (right). For larger mass splitting (right), the effect of Z -mediated s -channel cross sections arising due to χ^+ annihilation become negligible, and co-annihilation channels dominate increasing the relic density in the low DM mass regime within observed limits.

In Fig. 8, the variation of DM relic density is plotted with DM mass for two different mass splittings between χ^+ and ψ . In the left panel, the splitting is fixed at 1 GeV. For such a small splitting, the annihilation of the other dark sector particle χ^+ into SM fermions also contributes to the relic density along with the diagrams given in Fig. 2. All these additional channels being Z -mediated, we see the Z -resonance at $m_\psi = 45 \text{ GeV}$. After the resonance, these cross sections decrease with increase in m_ψ making the co-annihilation channels important. But if the mass splitting is made larger (5 GeV as shown in the right plot), then the effect of mediator annihilation, ie, the contribution of these Z -mediated diagrams becomes negligible compared to ψ co-annihilation and pair annihilation, so that even the low mass regime of m_ψ supports the correct relic density.

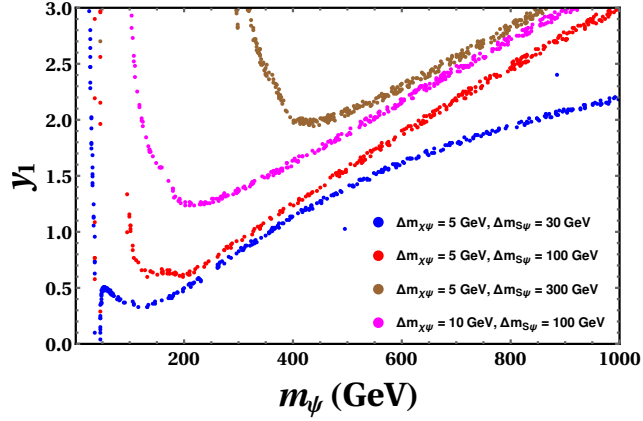


Figure 9: y_1 vs. m_ψ plot indicating the significance of the co-annihilation channels, with the mass splitting $\Delta m_{\chi\psi} = m_\chi - m_\psi = 5$ and 10 GeV, and for specific values of $\Delta m_{S\psi} = m_S - m_\psi$.

In Fig. 9, the variation of y_1 vs m_ψ is plotted with the mass splitting between ψ and χ^+ ($\Delta m_{\chi\psi}$) and the splitting between χ^+ and S^+ ($\Delta m_{S\psi}$) fixed at specific values. The dip at $m_\psi = 45$ GeV indicates a broad s -channel Z -resonance arising due to $\chi^+\chi^-$ mediator annihilation into SM fermions. The corresponding cross section being proportional to $e^{-2\Delta m_{\chi\psi}/m_\psi}$, it becomes irrelevant at mass splitting of 10 GeV, as indicated by the absence of such a dip in the deep pink curve. The co-annihilation channels, on the other hand, has a slightly more complex dependence on the masses. Considering the Feynman diagrams given in Fig. 2, there are three channels that could contribute. Two s -channel processes mediated by S^+ and a t -channel process mediated by χ^+ . Both the s -channel processes have S^+ in the final state as well. This brings in a tug of war between the resonant condition, $m_\chi + m_\psi = m_S$ and the favourable phase space for the lighter final state particles, consequently disfavouring the $\chi^+\psi \rightarrow S^+h$ channel. On the other hand, the other s -channel process with $S^+\gamma$ in the final state becomes significant around $m_S = m_\chi + m_\psi \sim 2m_\psi$. The t -channel process takes over at larger m_ψ , and the cross section slowly saturates. This is indicated in the plots at higher ψ masses. Heavier S^+ requires larger couplings to compensate for the diminishing effects of the propagator and narrowing phase space. This is clearly visible in the plots with larger $\Delta m_{S\psi}$ values. As soon as m_ψ becomes larger than m_S , the pair annihilation of ψ becomes dominant and the correct relic density is observed for m_ψ up to the TeV scale. Summing up, the solutions compatible with the required $y_1 \lesssim 10^{-5}$ is possible with highly degenerate regions with $\Delta m_{\psi\chi} \lesssim 5$ GeV in a narrow mass range of $m_\psi \sim \frac{m_Z}{2}$.

5 Collider signatures

The signatures of the model can be traced in colliders like the LHC through the gauge production and subsequent decay of the charged partner fermion, χ^+ and the charged scalar S^+ . We plot the cross section for pair production of χ^+ (σ_χ) at the 14 TeV LHC in Fig. 10a. At $m_\chi = 200$ GeV, the cross section is of the order of 100 fb, which falls down to 0.5 fb for $m_\chi = 1$ TeV. The charged scalar S^+ , on the other hand, has much smaller cross section (σ_S) of about 1 fb for $m_S = 100$ GeV, which reduces to about 0.1 fb for $m_S = 500$ GeV as seen from Fig. 10b. Subprocesses contributing to σ_χ and σ_S are $pp \rightarrow \chi^+\chi^-/S^+S^-$ via Z/γ s -channel diagrams. The decays of χ^+ and S^+ are controlled by the Yukawa couplings y_1 and y_2 . When both the couplings are large enough, the decays are instantaneous and

happens at the interaction point itself where the particles are produced. On the other hand, for small values of the couplings the decay width could be considerably smaller so that the decays happen away from the interaction point, leaving distinct signatures characteristic to such Long-Lived Particles (LLP). Indeed, such LLP arising in different contexts are actively studied for their signatures at LHC and other exclusively designed colliders like MATHUSLA in the past few years. Signatures typically include (i) *Displaced Vertex*, where the LLP decay within the detector, but away from the interaction point; (ii) *Heavy Stable Charged Particle (HSCP) tracks*, where charged LLP decaying outside the detector, leaving charged tracks similar to that of the muon, but with distinct features arising from slower speed and larger energy deposition along its flight through the materials of the detector or (iii) *Disappearing Tracks*, where an isolated track stopping before hitting the outer layers of the silicon tracker and without any associated energy deposition in the calorimeters or muon chamber. Experimental searches by CMS [48–50], ATLAS [54, 57–59] and LHCb [61–63] considered long-lived neutral scalar decaying in the calorimeter into pair of jets, looking for displaced vertex with negative results leading to constraints on the masses of the corresponding LLP. Considering a gauge-mediated supersymmetry breaking scenario, CMS [52] considered non-prompt jets arising from the decay of gluino to gluons and gravitinos, where the gluon jet emerges from a displaced vertex within the tracker. HSCP search by ATLAS [55, 56] and CMS [53] looking for possible candidates in the supersymmetric scenarios have obtained mass limits on the so-called R -hadrons (long-lived gluinos or squarks), staus and charginos. Long time of flight along with presence of anomalously high energy deposits in the silicon detector is basically considered as the signature of the HSCP. Reference [56] has used the ionisation information from the pixel subsystems of ATLAS detector to probe the HSCP modelled after R -hadron. CMS [51, 86] and ATLAS [60] considered disappearing tracks arising from chargino decay to neutralinos and a low-momentum pion, where the neutralino is nearly mass degenerate with the chargino, resulting in its long decay time. A recent report on the strategies that may be adopted in searching for LLP at colliders like the LHC discussing simplified models, experimental signatures, details of the backgrounds and possible requirements of detector upgrades presented in Ref. [47]. A comprehensive analysis of LLP arising in FIMP like scenario is presented in Ref. [81], where the authors have described possible signatures of a long-lived charged fermion decaying into the SM charged lepton and scalar DM candidate. Considering fermionic dark matter as a mixture of $SU(2)_L$ singlet and doublet LLP signatures at the LHC are studied in Ref. [91]. Charged dark doublet scalar decaying into fermionic FIMP and charged leptons are considered in [92]. In addition to the possible searches at the LHC, there are proposals for dedicated detectors like MATHUSLA [79, 80], which can potentially look for long-lived neutral particles decaying to two jets or charged leptons outside the LHC detectors. These surface detectors are located so as to look for long-lived neutral particles originating from the interaction point, decaying in its volume into two identifiable jets or leptons.

Many of the signatures discussed above would be present in the scenario discussed in this work. In this case, the charged dark fermion, χ^+ , the Z_2 -even charged scalar, S^+ and the heavy neutrino N are all possible candidates of LLP. The specific signatures of the LLP will depend on many aspects. A particular feature pertaining to the model presented in our case is the possibility of *multiple LLP signatures* arising through the cascade decay of the kind $LLP1 \rightarrow LLP2 + X$. In the present case, this is possible whenever the 2-body decay of χ^+ is allowed. In such case, χ^+ decays to an on-shell S^+ , which itself could be an LLP when its decay is slow, enabled by small y_2 . However, for large enough y_2 , S^+ decays quickly

enough without leaving any displaced vertex. In that case, the LLP signature of χ^+ is the standard case of usual single LLP. Interesting signature of multiple LLP processes are not investigated in detail in the literature. To illustrate this we shall take a specific case with $c\tau(\chi) = \frac{c}{\Gamma_\chi} \leq 50$ cm and $c\tau(S^+) \sim 1 - 10$ m, with the first displaced vertex falling in the Inner Detector, followed by the second one (that of S^+ decay) falling in the Calorimeter or Muon Spectrometer. The first displaced vertex will leave a kink on the track, with the accompanying ψ invisible. Distinguishability of this kink depends on the masses and energy of the particles, apart from the granularity of the detectors. While we recognise the fact that such possibilities are complex to probe, with precision of a few microns on position in the pixel detector, and high precision calorimeters it is worth exploring the possibilities. In addition to charged χ^+ and S^+ , we have the presence of heavy neutral fermions that couple to the charged leptons through the standard Higgs boson. The Yukawa coupling corresponding to this interaction is small, making N almost always stable within the detector. However, for N heavier than 125 GeV, Yukawa couplings of the order of 10^{-8} would lead to its decay within the detector.

We shall consider some preliminary numerical analysis of the above long-lived situations with χ^+ , S^+ and N separately in the following subsections.

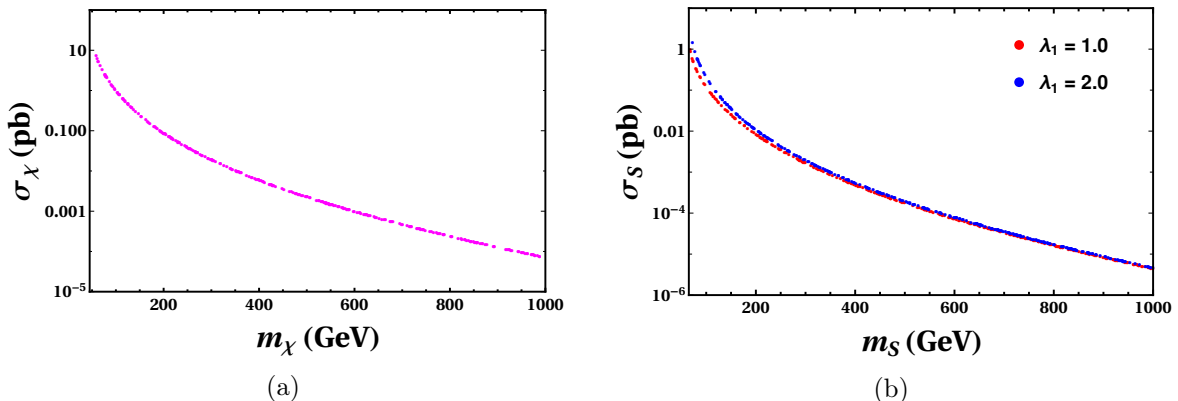


Figure 10: Production cross section of $\chi^+\chi^-$ (a) and S^+S^- (b) pair at 14 TeV LHC for different values m_χ and m_S , respectively.

5.1 Long-lived charged fermion, χ^+

The conditions on χ^+ arising from the dark matter considerations depend on its mass and nature of decay. In the kinematic regions where $m_\chi > m_S + m_\psi$, the decay of χ^+ is dictated by the Yukawa coupling, y_1 , the Feynman diagram for which is given in Fig. 1a. From Fig. 3 it is clear that χ^+ lighter than about 200 GeV is not favoured in this case. The compatible couplings are restricted to $10^{-13} \leq y_1 \leq 10^{-8}$, leading to $c\tau$ in the range of interest of LHC for the larger limits of the coupling. Fig. 11a gives the decay lengths for a range of m_χ and typical values of the coupling, for fixed masses of $m_\psi = 1$ GeV and $m_S = 65$ GeV. We have checked the sensitivity with varying m_ψ and m_S , and found that the decay length remains in the same order of magnitude for a large range of these masses. Keeping all other parameters the same, the dependence of $c\tau$ on m_χ is minimal, allowing a wide range of the mass values to be accessible as LLPs at the LHC. We tabulate the decay lengths for typical values of m_χ fixing $y_1 = 10^{-8}$ in Table 8. Note that the decay width is proportional to y_1^2 in this case, and

therefore, $c\tau$ for a specific y_1 value can be obtained from what is quoted in table by using the scaling factor $10^{-16}/y_1^2$. For example, by choosing a slightly larger y_1 value the decay length can be brought down to the centimetre range, which is relevant to the Inner Detector of LHC experiments. At the same time, couplings smaller than 10^{-8} leads to χ^+ escaping the detector without decaying, leaving charged track in all sections of the detector, very similar to that of the μ tracks, but with larger energy deposition owing to it being heavier [76, 81]. In addition, its time of flight will be larger than that of muon as it would be slower than muons.

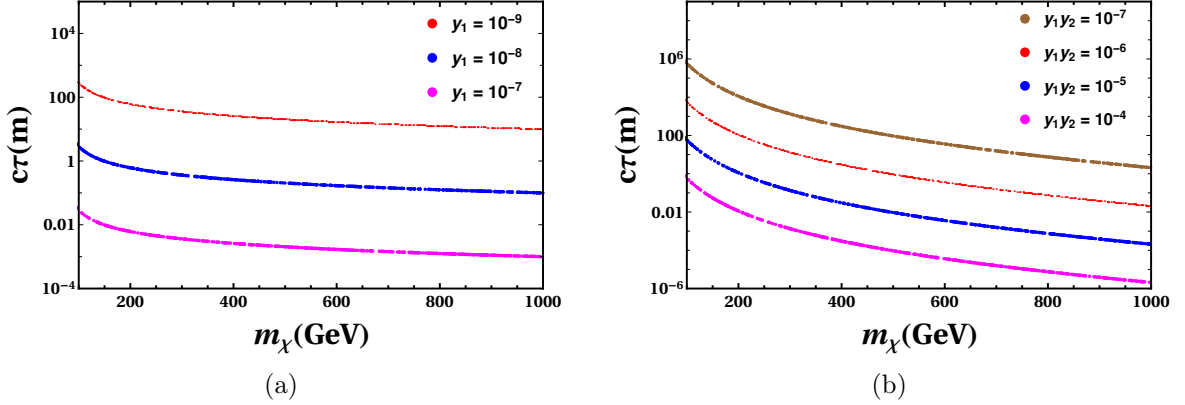


Figure 11: Decay length vs. mass of χ^+ for different couplings corresponding to (a) 2-body and (b) 3-body decay of χ^+ . The neutral particle masses are $m_\psi = 1$ GeV and $m_N = 30$ GeV, while the charged scalar masses m_S are 65 GeV for case (a) and 1 TeV for case (b).

y_1	m_χ	m_ψ	m_S	$c\tau$ (m)
10^{-8}	200	130	65	55
		65	65	72
		65	130	110
	1000	900	65	63
		65	65	88
		65	900	710

(a)

$y_1 y_2$	m_χ	m_ψ	m_S	$c\tau$ (m)
10^{-6}	40	1	65	166
	100	60	120	69
	500	400	300	1
		400	1000	155
	1000	800	800	1
		900	500	8
		300	800	0.002

(b)

Table 8: Decay length ($c\tau$) of χ^+ in meters for typical masses of ψ and S^+ and at a fixed value of the coupling. All masses are in GeV. Heavy neutrino mass is set to $m_N = 30$ GeV.

Moving on to the case of $m_\chi < m_S + m_\psi$, the two-body decay is kinematically disallowed and the three body decay $\chi^+ \rightarrow \psi N \ell^+$ is controlled by the product $y_1 y_2$ and mediated by a virtual S^* , as shown in the Feynman diagram in Fig. 1b. In this case, χ^+ can be lighter than 100 GeV as seen from Fig. 4, with the product of the couplings mostly range between 10^{-10} and 10^{-6} . With conditions of mass splitting satisfied for enhanced co-annihilation, possibilities with larger couplings even up to 10^{-5} are not rare, and may even reach up to 10^{-4} albeit with less probability, as presented in Table 5. In Fig. 11b the decay length $c\tau$

is plotted against m_χ for exemplary values of the relevant coupling combination, keeping $m_\psi + m_N + m_\ell < m_\chi < m_\psi + m_S$ so as to focus on the 3-body decay. The dependence on the mass here is stronger than that in the 2-body decay case discussed above. For the entire mass range of $m_\chi = 40$ GeV to large values of $m_\chi = 1000$ GeV it is possible to have χ^+ decaying within the Inner Detector or the Calorimeters, or even decay outside the detectors, leaving a LLP signature. Table 8b shows the decay lengths for some specific benchmark points relevant to the LHC.

5.2 Long-lived charged scalar, S^+

Turning to the case of S^+ , its decay length is decided purely by the strength of y_2 . For the freeze-in solution of dark matter, we needed $y_1 \lesssim 10^{-8}$ so as to be compatible with the observed relic density. The charged scalar, S^+ is mostly produced through gauge mediation, with a small contribution from the Higgs mediated process enabled by the quartic coupling λ_1 . When the coupling y_1 is of the order of unity, on the other hand, as required in the case of freeze-out mechanism to generate the dark matter relic density, χ^+ would decay instantly as it is produced. It will decay to $S^+\psi$, with S^+ further decaying and ψ missing. The cross section for this is given in Fig. 10b against m_S at 14 TeV LHC. The decay of S^+ is decided by the Yukawa coupling y_2 . The decay width is given by

$$\Gamma_{S^+ \rightarrow N\ell} = \frac{y_2^2}{16\pi m_S^3} (m_S^2 - m_N^2 - m_\ell^2) [\{m_S^2 - (m_N + m_\ell)^2\} \{m_S^2 - (m_N - m_\ell)^2\}]^{\frac{1}{2}}. \quad (5.1)$$

In Fig. 12 we plot the decay length of S^+ against m_S for specific choices of the relevant Yukawa coupling, y_2 . Considering this to be of the order of $10^{-8} - 10^{-10}$ makes it decay within the LHC detector, but with a measurable delay from its production so as to distinguish it from other particles which decay instantly. The signatures depend on the actual decay width. For $y_2 \sim 10^{-8} - 10^{-9}$ it leave a displaced vertex in the Inner Detector, whereas weaker couplings would make it decay within the Calorimeters or even in the muon detectors. Beyond $y_1 \sim 10^{-10}$ will see S^+ escaping the LHC detectors without decaying, but leaving a clear charged particle track in all sectors. Similar to the case of χ^+ discussed above, this can perhaps be distinguished from the muon tracks, owing to its heavy nature and slower speed. It is also interesting that the mass splitting between S^+ and N dictates the signatures of S^+ at the collider. If the splitting is small, a soft lepton will be produced in the final state, leaving disappearing tracks. On the other hand, if the splitting is large, then very likely a kink will be seen in the typical charged track signal. The cross-sections and decay widths of S^+ for selected benchmark points are given in Table 9 for some typical benchmark points which satisfy the relic density bound.

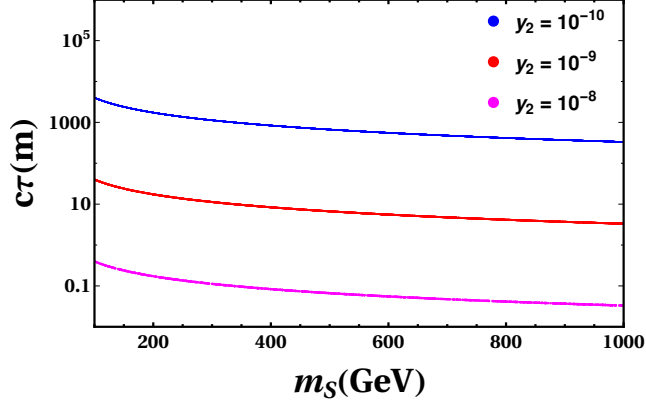


Figure 12: Decay length vs. mass of long lived particle (S^+) for different couplings. m_N is fixed at 30 GeV.

	m_ψ	m_S	m_χ	y_1	Ωh^2	$\sigma_{pp \rightarrow S^+ S^-}$ (pb)	$\Gamma_{S^+ \rightarrow N \ell}$ (GeV)	$c \tau$ (m)
BP 1	56	165	473	7.53×10^{-13}	0.12	0.0144	9.21×10^{-18}	21.5
BP 2	101	77	613	1.18×10^{-13}	0.118	0.2441	3.3×10^{-18}	60.0
BP 3	225	188	228	0.01	0.12	0.0088	1.07×10^{-17}	18.5
BP 4	150	127	154	0.05	0.119	0.0376	6.76×10^{-18}	29.5

Table 9: Values of benchmark points considered in this paper for the production cross section (at 14 TeV LHC) and decay of the charged scalar S^+ . DM relic density is achieved through either freeze-in (2 body) or freeze-out. All masses are in GeV. For all points, $m_N = 30$ GeV and $y_2 = 10^{-9}$.

5.3 Long-lived neutral fermion, N

The neutral heavy fermion, N , decays through $N\nu h$ interaction, where ν is the SM neutrino and h is the SM Higgs boson. The strength of this interaction is decided by the Yukawa coupling y_N , which also decides the neutrino mass through the seesaw mechanism. As discussed in the introduction, this coupling is required to be $\sim 10^{-8}$ for m_N considered in our discussion. In addition, for $m_N < 125$ GeV it cannot decay to an on-shell Higgs boson, further slowing down the decay. Therefore, N (of mass in the 100 GeV range or lighter) decays much beyond the LHC detectors, consequently leaving missing energy signature, like the SM neutrinos. Dedicated detectors like the MATHUSLA [79] placed beyond the LHC detector complex could capture the signatures of such long lived particles. This surface detector is typically prepared to identify decay of LLP into a pair of charged particles, which are detected by its multi-layer trackers. However, notice that N decays to neutrino and Higgs boson. With the missing energy, it will be difficult to correlate the event as originating from the interaction point. Different techniques like time of flight information may need to be made use of, requiring close talks between the CMS/ATLAS and MATHUSLA detectors. On the other hand, for $m_N \gtrsim 130$ GeV, N can have decay length within the CMS/ATLAS detector, and can in principle be probed through the displaced vertex study. Again, the typical search strategies adopted in the case of displaced vertex studies of ATLAS and CMS will not work in this case.

It may be required to look for reconstructed Higgs (produced almost at rest, especially when N is nearly degenerate with Higgs) originating from a displaced vertex along with associated missing transverse momentum with respect to the direction of the interaction point could be a possible signature. Although we have not considered heavier N for our analysis, in order to

m_N (GeV)	Γ_N (GeV)	$c\tau$ (m)
100	1.53×10^{-22}	1.3×10^6
120	7.53×10^{-22}	2.8×10^5
128	4.09×10^{-19}	480.5
130	1.1×10^{-18}	179
135	4.1×10^{-18}	48.05
150	2.09×10^{-17}	9.42
200	1.1×10^{-16}	1.79

Table 10: Decay width and decay length of N . $y_N = 10^{-8}$ in all cases. It is to be noted that the order of Γ_N changes substantially for $m_N \geq 125$ GeV, which implies the onshell production of SM Higgs.

get the same relic density, the increase in m_N in the decay width of χ can be compensated by larger $y_1 y_2$.

Finally, we may consider these search options in the proposed e^+e^- colliders like CLIC with sufficient centre of mass energy to produce the charged particle, χ^+ and S^+ . The search strategies in this case would be very similar to that mentioned above in the case of the LHC. Notice that the production being electroweak process, cross section in this case will be comparable with the LHC. On the other hand, the clean environment and fixed centre of mass energy can be of great advantage in the leptonic colliders. We shall defer a detailed study to a future publication.

6 Conclusion

Providing a viable dark matter candidate, yet compatible with all the experimental observations is one of the major challenges of particle physics today. In the popular WIMP scenario, weakly interacting dark matter particles produced thermally in abundance is depleted with large enough annihilations to achieve the observed relic density as they decouple and freeze out. In most models of WIMP the basic interaction that leads to such annihilations is the same as that is relevant in the direct detection experiments based on their elastic scattering from nuclei. Presently, the direct detection experiments have constrained these couplings to the extent that it becomes quite difficult to accommodate the required annihilation cross section. This has led many researchers to favour an alternate mechanism, whereby very feebly interacting massive particles are slowly produced to build up the relic density of the dark matter. In this FIMP scenario, usually, a thermally produced partner particle decays very slowly to the dark matter particle.

In this work we consider a gauge singlet fermionic FIMP dark matter, ψ and an isospin singlet charged fermion, χ^+ as its partner particle. The stability of the dark matter particle is ensured by imposing a Z_2 symmetry under which both χ and ψ are odd, while all other particles are even. Gauge produced χ^+ decays through its Yukawa coupling (y_1) to ψ and

another newly introduced isospin singlet charged scalar S^+ . For very small values of this Yukawa coupling, the dark matter density will be slowly built up. Our analysis shows that for $10^{-13} \leq y_1 \leq 10^{-8}$ a wide range of DM mass $1 \text{ GeV} \leq m_\psi \leq 600 \text{ GeV}$ is viable for partner mass of 100 - 1000 GeV. The presence of S^+ and the Yukawa coupling (y_2) enabling its decay to a heavy neutral fermion and the charged SM leptons, add an entirely new dimension to the dynamics compared to what is usually discussed in the literature. The signatures here include a slowly decaying long-lived particle, as well as the dark matter particle itself. Under favourable conditions, the partner particles can be produced in sufficient amounts at colliders like the LHC, which then will decay away from the interaction point, but within the detector, leaving distinct signatures compared to many exotic particle searches. The typical coupling (relevant to the decay) required for this is $\sim 10^{-9}$, which in the usual FIMP scenarios discussed in the literature require very light dark matter candidates (keV - MeV). In the present scenario we discussed, the presence of y_2 , which can be independent of the dark matter considerations makes it possible to have both χ^+ and S^+ to be a long lived particles that could be searched at the LHC, for a large range of its mass. When the kinematic condition $m_\chi > m_\psi + m_S$ is not met, χ^+ decays through off-shell S^+ to $N\ell^+\psi$. This decay is controlled by a combination of y_1 and y_2 . With y_1 within a restricted range, y_2 can be arranged so that the delayed decay of χ^+ to the DM candidate ψ adds significantly to its number density. This is a new feature of the dark matter dynamics that is comparatively less explored in the literature. This intermingling of slow production leading to freeze-in and annihilation followed by freeze-out opens up a large region of the parameter space, otherwise unavailable when these mechanisms are considered separately. We have discussed the details of this in Section 3.2, where the importance of annihilation process is clearly established. In sharp contrast to the usual freeze-in plus LLP scenario, the DM mass range that is compatible in the present case is from a few GeV to TeV. While the usual HSCP scenario arises in certain parameter regions, there are other distinct features requiring modified search strategy at LHC/MATHUSLA detectors as summarised below.

1. Having two charged LLP 's, it is possible to have $LLP1 \rightarrow LLP2 + \cancel{E}$, with $LLP2$ decaying outside the detector. With large enough missing energy, this can lead to a HSCP track with a kink at the first decay vertex.
2. $LLP1 \rightarrow LLP2 + MET \rightarrow SM + MET$. Within favourable parameter regions, this can lead to sufficiently large disappearing track, with a kink at the first decay vertex.
3. The neutral LLP decay to Higgs boson and neutrino ($N \rightarrow h\nu$). With h further decaying to $b\bar{b}$, this could lead to two jets with displaced vertex, and having invariant mass around Higgs mass, within ATLAS/CMS or MATHUSLA. The reconstructed Higgs momentum will not point to the interaction point owing to large associated missing energy of the undetected neutrino.

We have explored various possibilities, and show that for m_ψ starting from 1 GeV all the way up to 1000 GeV and beyond, almost the entire range of theoretically allowed coupling values and a large range of masses of other particles are compatible with the observations. The collider phenomenology in this region of parameter space may not feature any long-lived particle. On the other hand, presence of two exotic charged particles, one fermion and one scalar will add rich phenomenology, which will be explored in detail in a different work. For easy reference, we have summarised the conclusions in a qualitative way for different ranges of the relevant couplings in Table 11.

DM scenario	couplings			LLP	collider signature
	y_1	y_2	$y_1 y_2$		
Freeze-in via 2 body decay	$10^{-13} \lesssim y_1 \lesssim 10^{-9}$	$10^{-10} \lesssim y_2 \lesssim 10^{-7}$	small	χ^+ S^+	charged track displaced vertex, charged track
Freeze-in via 3 body decay	$\lesssim 10^{-8}$	$10^{-3} \lesssim y_2 \lesssim 1$	$10^{-11} \lesssim y_1 y_2 \lesssim 10^{-8}$	χ^+	charged track
thermal production + non-thermal production through χ^+ decay (dominant)	$10^{-8} \lesssim y_1 \lesssim 10^{-7}$	$10^{-3} \lesssim y_2 \lesssim 1$	$10^{-11} \lesssim y_1 y_2 \lesssim 10^{-7}$	χ^+	charged track
Freeze-out	~ 1	$\lesssim 10^{-7}$	$\lesssim 10^{-4}$	χ^+ S^+	charged track, displaced vertex displaced vertex, charged track
Freeze-out	~ 1	~ 1	~ 1	-	-

Table 11: Table showing the possible DM scenarios and the limits on the coupling from relic density and collider requirements. LLP possibilities and signatures are also mentioned.

Finally, we point the attention of the reader to the presence of heavy neutral fermion inducing type-I seesaw mechanism providing a way to generate light neutrino mass within the same framework, as an added feature of the model.

A Boltzmann Equations

The dark matter particle ψ when produced with slow decay of χ^+ , but with a rate that results in sufficiently large number density of ψ before freezing-in presents a novel feature as discussed towards the end of Section 3.2. With sufficiently large value of the relevant coupling, y_1 , the thermal production and pair annihilation become significant, leading to freeze-out. The two limiting cases are (i) with y_1 is small enough so that only the production through χ^+ decay is relevant, and (ii) with y_1 large enough so that the thermal production and subsequent freeze-out scenario are relevant. The Boltzmann Equation controlling the yield in this case depends on the annihilation cross section of ψ along with the decay rate of χ^+ as given by

$$\frac{dY_\psi}{dx} = \sqrt{\frac{45}{4\pi^3 G}} \frac{x}{m_\psi^2} \frac{\sqrt{g_*(T)}}{g_s(T)} (\langle \Gamma_{\chi \rightarrow \psi X} \rangle Y_{\chi_{eq}}) - \sqrt{\frac{\pi}{4\pi G}} \frac{m_\psi}{x^2} \sqrt{g_*(T)} \langle \sigma v \rangle_\chi (Y_\psi^2 - Y_{\psi_{eq}}^2),$$

with $Y_{\chi_{eq}}$ and $Y_{\psi_{eq}}$ are the equilibrium number densities for χ^+ and ψ respectively, $x = m_\psi/T$, where T is the photon temperature. Notice that in the standard freeze-in case x is defined in terms of the mass of the decaying particle (χ^+ in our case). However, what is relevant in the present case is the final freeze-out, and therefore we have considered $x = \frac{m_\psi}{T}$, appropriately redefining other factors.

$$\sqrt{g_*(T)} \simeq \frac{g_s(T)}{\sqrt{g_\rho(T)}}$$

where g_s and g_ρ are the degrees of freedom corresponding to entropy and energy density of the Universe.

$$\langle \Gamma_{\chi^+ \rightarrow \psi X} \rangle = \Gamma_{\chi^+ \rightarrow \psi X} \frac{K_1(x')}{K_2(x')}$$

$x' = m_\chi/T$, K_1 and K_2 are modified Bessel functions and $\Gamma_{\chi^+ \rightarrow \psi X}$ represents the decay width of χ^+ to ψ and X , where X denotes S^+ in case of 2 body and N and l^+ for 3 body decay of χ^+ . $\langle \sigma v \rangle_{\chi^+}$ denotes the thermal average of all possible pair annihilation and coannihilation cross-sections of ψ .

The relic density is related to the yield through the standard relation,

$$\Omega_\psi h^2 = 2.75 \times 10^8 m_\psi Y_\psi(T_0), \quad (\text{A.1})$$

where T_0 is the present temperature of the universe.

B Constraint from $H \rightarrow \gamma\gamma$

The Higgs boson has a direct quartic coupling with the new charged scalar, S^+ ,

$$\mathcal{L} \ni \lambda_1 S^\dagger S H^\dagger H. \quad (\text{B.1})$$

The trilinear coupling arising from this after the electroweak symmetry breaking results in S^+ contribution to $H \rightarrow \gamma\gamma$ at the leading order through the triangle diagram. Including this contribution from S^+ , the diphoton decay width is given by [93, 94]

$$\Gamma(H \rightarrow \gamma\gamma) = \frac{\alpha^2 m_H^3}{256 \pi^3 v^2} \left| F_W + \sum_f N_{cf} Q_f^2 F_f + \lambda_1 v F_S \right|^2, \quad (\text{B.2})$$

where

$$F_W = 2 + 3\tau_W [1 + (2 - \tau_W) f(\tau_W)], \quad (\text{B.3})$$

$$F_f = -2\tau_f [1 + (1 - \tau_f) f(\tau_f)], \quad (\text{B.4})$$

$$F_S = \tau_S [1 - \tau_S f(\tau_S)], \quad (\text{B.5})$$

with $\tau_i = \frac{4m_i^2}{m_h^2}$ and

$$f(\tau) = \begin{cases} \text{ArcSin}^2(1/\sqrt{\tau}), & \text{for } \tau \geq 1 \\ -\frac{1}{4} \ln \left(\frac{1+\sqrt{1-\tau}}{1-\sqrt{1-\tau}} \right) - i\pi, & \text{for } \tau < 1. \end{cases} \quad (\text{B.6})$$

With $m_S = 150$ GeV, we have

$$\Gamma(H \rightarrow \gamma\gamma) \sim 0.25 \text{ (keV)} (6.54 - 90.5 \lambda_1)^2. \quad (\text{B.7})$$

C Constraint from Invisible Higgs decay

Higgs boson does not have direct coupling to the dark matter, ψ . However, $H \rightarrow \psi\psi$ is

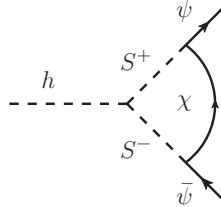


Figure 13: Feynman diagram contributing to the invisible Higgs decay through $H \rightarrow \psi\psi$.

possible through the one loop diagram as in Fig. 13. This contribution to the invisible decay of the Higgs is given by [95]

$$\Gamma(H \rightarrow \psi\psi) = \frac{m_H}{2\pi} \left[1 - \frac{4m_\psi^2}{m_H^2} \right]^{3/2} |g_V|^2, \quad (\text{C.1})$$

with

$$g_V = \frac{\lambda_1 y_1^2 v}{32\pi^2} \left[2m_\psi C_1(m_\psi^2, m_H^2, m_\psi^2, m_\chi, m_S, m_S) - m_\chi C_0(m_\psi^2, m_H^2, m_\psi^2, m_\chi, m_S, m_S) \right],$$

where C_i are the relevant Passarino-Veltman loop functions. With all new particle masses around GeV-TeV scale, $\Gamma(H \rightarrow \psi\bar{\psi}) \sim \mathcal{O}(10^{-6})$ for the couplings $y_1 \sim 1$ and $\lambda_1 \sim 0.01$ which is negligible compared to the standard contributions.

D Direct Detection Constraints

There are two sets of Feynman diagrams with photon and Z mediation, as in Fig. 14. The

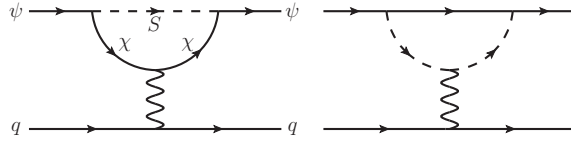


Figure 14: One-loop diagrams that contribute to dark matter - nucleon scattering. Notice that there are no tree-level contributions.

spin-independent direct detection cross section is given by [96]

$$\sigma_{\text{SI}}^{\psi\chi} = \frac{16}{\pi} \frac{m_\psi^3 m_p^3}{m_\psi + m_p} |c_{VV}^q|^2, \quad (\text{D.1})$$

where m_p is the proton mass. The relevant Wilson coefficients are given by

$$\begin{aligned} c_{VV}^q = & -\frac{\alpha_{\text{em}}}{24\pi x_\psi^4} \frac{1}{m_S^2} Q Q_q y_1^2 \left[\left(-3x_\psi^6 + 6x_\psi^5 x_\chi + 12x_\psi x_\chi (1-x_\chi^2)^2 + 8(1-x_\chi^2)^3 + 2x_\psi^4 (5+x_\chi^2) \right. \right. \\ & \left. \left. - 6x_\psi^3 x_\chi (1+3x_\chi^2) - 3x_\psi^2 (5-2x_\chi^2-3x_\chi^4) \right) \frac{g(x_\psi, x_\chi)}{1-(x_\psi-x_\chi)^2} + \frac{2x_\psi^2 (4-3x_\psi^2+6x_\psi x_\chi-4x_\chi^2)}{1-(x_\psi-x_\chi)^2} \right. \\ & \left. + (8+x_\psi^2-4x_\psi x_\chi-8x_\chi^2) \ln x_\chi \right]. \end{aligned} \quad (\text{D.2})$$

The loop function in terms of the mass ratios $x_\psi \equiv \frac{m_\psi}{m_S}$ and $x_\chi \equiv \frac{m_\chi}{m_S}$ is given by

$$g(x_\psi, x_\chi) = \frac{\ln \left(1 - x_\psi^2 + x_\chi^2 + \sqrt{x_\psi^4 + (1-x_\chi^2)^2 - 2x_\psi^2(1+x_\chi^2)} \right) - \ln(2x_\chi)}{\sqrt{x_\psi^4 + (1-x_\chi^2)^2 - 2x_\psi^2(1+x_\chi^2)}}. \quad (\text{D.3})$$

Acknowledgments

PP and SC thank DST-SERB, India for the research project grant EMR/2015/000333, and the DSTFIST grant SR/FST/PSII-020/2009 for offering the computing resources needed by this work. SC would like to acknowledge fruitful discussions with Amit Dutta Banik and Rashidul Islam and thank MHRD, Govt. of India for research fellowship. We also thank the British Council, India for sponsoring the visit of VM to IIT Guwahati during which the collaboration was initiated.

References

- [1] PLANCK collaboration, N. Aghanim et al., *Planck 2018 results. VI. Cosmological parameters*, [1807.06209](#).
- [2] G. Jungman, M. Kamionkowski and K. Griest, *Supersymmetric dark matter*, *Phys. Rept.* **267** (1996) 195 [[hep-ph/9506380](#)].
- [3] XENON collaboration, E. Aprile et al., *First Dark Matter Search Results from the XENON1T Experiment*, *Phys. Rev. Lett.* **119** (2017) 181301 [[1705.06655](#)].
- [4] LUX collaboration, D. S. Akerib et al., *Results from a search for dark matter in the complete LUX exposure*, *Phys. Rev. Lett.* **118** (2017) 021303 [[1608.07648](#)].
- [5] LUX collaboration, D. S. Akerib et al., *Limits on spin-dependent WIMP-nucleon cross section obtained from the complete LUX exposure*, *Phys. Rev. Lett.* **118** (2017) 251302 [[1705.03380](#)].
- [6] PANDAX-II collaboration, X. Cui et al., *Dark Matter Results From 54-Ton-Day Exposure of PandaX-II Experiment*, *Phys. Rev. Lett.* **119** (2017) 181302 [[1708.06917](#)].
- [7] DEAP-3600 collaboration, P. A. Amaudruz et al., *First results from the DEAP-3600 dark matter search with argon at SNOLAB*, *Phys. Rev. Lett.* **121** (2018) 071801 [[1707.08042](#)].
- [8] SUPERCDMS collaboration, R. Agnese et al., *Results from the Super Cryogenic Dark Matter Search Experiment at Soudan*, *Phys. Rev. Lett.* **120** (2018) 061802 [[1708.08869](#)].
- [9] SUPERCDMS collaboration, R. Agnese et al., *New Results from the Search for Low-Mass Weakly Interacting Massive Particles with the CDMS Low Ionization Threshold Experiment*, *Phys. Rev. Lett.* **116** (2016) 071301 [[1509.02448](#)].
- [10] CRESST collaboration, G. Angloher et al., *Results on light dark matter particles with a low-threshold CRESST-II detector*, *Eur. Phys. J.* **C76** (2016) 25 [[1509.01515](#)].
- [11] G. Arcadi, M. Dutra, P. Ghosh, M. Lindner, Y. Mambrini, M. Pierre et al., *The waning of the WIMP? A review of models, searches, and constraints*, *Eur. Phys. J.* **C78** (2018) 203 [[1703.07364](#)].
- [12] CRESST collaboration, G. Angloher et al., *Results on MeV-scale dark matter from a gram-scale cryogenic calorimeter operated above ground*, *Eur. Phys. J.* **C77** (2017) 637 [[1707.06749](#)].
- [13] NEWS-G collaboration, Q. Arnaud et al., *First results from the NEWS-G direct dark matter search experiment at the LSM*, *Astropart. Phys.* **97** (2018) 54 [[1706.04934](#)].
- [14] PICO collaboration, C. Amole et al., *Dark Matter Search Results from the PICO-60 C₃F₈ Bubble Chamber*, *Phys. Rev. Lett.* **118** (2017) 251301 [[1702.07666](#)].
- [15] GAMBIT collaboration, P. Athron et al., *Status of the scalar singlet dark matter model*, *Eur. Phys. J.* **C77** (2017) 568 [[1705.07931](#)].
- [16] L. Lopez Honorez, E. Nezri, J. F. Oliver and M. H. G. Tytgat, *The Inert Doublet Model: An Archetype for Dark Matter*, *JCAP* **0702** (2007) 028 [[hep-ph/0612275](#)].

- [17] T. Hambye, F. S. Ling, L. Lopez Honorez and J. Rocher, *Scalar Multiplet Dark Matter*, *JHEP* **07** (2009) 090 [[0903.4010](#)].
- [18] L. Lopez Honorez and C. E. Yaguna, *The inert doublet model of dark matter revisited*, *JHEP* **09** (2010) 046 [[1003.3125](#)].
- [19] A. Belyaev, G. Cacciapaglia, I. P. Ivanov, F. Rojas-Abatte and M. Thomas, *Anatomy of the Inert Two Higgs Doublet Model in the light of the LHC and non-LHC Dark Matter Searches*, *Phys. Rev.* **D97** (2018) 035011 [[1612.00511](#)].
- [20] A. Goudelis, B. Herrmann and O. StÃl, *Dark matter in the Inert Doublet Model after the discovery of a Higgs-like boson at the LHC*, *JHEP* **09** (2013) 106 [[1303.3010](#)].
- [21] P. Poulose, S. Sahoo and K. Sridhar, *Exploring the Inert Doublet Model through the dijet plus missing transverse energy channel at the LHC*, *Phys. Lett.* **B765** (2017) 300 [[1604.03045](#)].
- [22] W. Chao, *A Three Higgs Doublet Model for Fermion Masses*, *Commun. Theor. Phys.* **66** (2016) 340 [[1201.0364](#)].
- [23] V. Keus, S. F. King and S. Moretti, *Three-Higgs-doublet models: symmetries, potentials and Higgs boson masses*, *JHEP* **01** (2014) 052 [[1310.8253](#)].
- [24] Y. G. Kim and K. Y. Lee, *The Minimal model of fermionic dark matter*, *Phys. Rev.* **D75** (2007) 115012 [[hep-ph/0611069](#)].
- [25] Y. G. Kim, K. Y. Lee and S. Shin, *Singlet fermionic dark matter*, *JHEP* **05** (2008) 100 [[0803.2932](#)].
- [26] S. Baek, P. Ko and W.-I. Park, *Search for the Higgs portal to a singlet fermionic dark matter at the LHC*, *JHEP* **02** (2012) 047 [[1112.1847](#)].
- [27] S. Bhattacharya, N. Sahoo and N. Sahu, *Minimal vectorlike leptonic dark matter and signatures at the LHC*, *Phys. Rev.* **D93** (2016) 115040 [[1510.02760](#)].
- [28] O. Lebedev, H. M. Lee and Y. Mambrini, *Vector Higgs-portal dark matter and the invisible Higgs*, *Phys. Lett.* **B707** (2012) 570 [[1111.4482](#)].
- [29] G. Arcadi, A. Djouadi and M. Raidal, *Dark Matter through the Higgs portal*, [1903.03616](#).
- [30] L. Bian, T. Li, J. Shu and X.-C. Wang, *Two component dark matter with multi-Higgs portals*, *JHEP* **03** (2015) 126 [[1412.5443](#)].
- [31] A. DiFranzo and G. Mohlabeng, *Multi-component Dark Matter through a Radiative Higgs Portal*, *JHEP* **01** (2017) 080 [[1610.07606](#)].
- [32] S. Bhattacharya, E. Ma and D. Wegman, *Supersymmetric left-right model with radiative neutrino mass and multipartite dark matter*, *Eur. Phys. J.* **C74** (2014) 2902 [[1308.4177](#)].
- [33] S. Bhattacharya, P. Poulose and P. Ghosh, *Multipartite Interacting Scalar Dark Matter in the light of updated LUX data*, *JCAP* **1704** (2017) 043 [[1607.08461](#)].
- [34] A. Ahmed, M. Duch, B. Grzadkowski and M. Iglicki, *Multi-Component Dark Matter: the vector and fermion case*, [1710.01853](#).
- [35] S. Bhattacharya, P. Ghosh, T. N. Maity and T. S. Ray, *Mitigating Direct Detection Bounds in Non-minimal Higgs Portal Scalar Dark Matter Models*, *JHEP* **10** (2017) 088 [[1706.04699](#)].
- [36] S. Bhattacharya, A. Drozd, B. Grzadkowski and J. Wudka, *Two-Component Dark Matter*, *JHEP* **10** (2013) 158 [[1309.2986](#)].
- [37] S. Chakraborti and P. Poulose, *Interplay of Scalar and Fermionic Components in a Multi-component Dark Matter Scenario*, [1808.01979](#).
- [38] S. Chakraborti, A. Dutta Banik and R. Islam, *Probing Multicomponent Extension of Inert Doublet Model with a Vector Dark Matter*, [1810.05595](#).

- [39] S. Bhattacharya, P. Ghosh and N. Sahu, *Multipartite Dark Matter with Scalars, Fermions and signatures at LHC*, *JHEP* **02** (2019) 059 [[1809.07474](#)].
- [40] L. J. Hall, K. Jedamzik, J. March-Russell and S. M. West, *Freeze-In Production of FIMP Dark Matter*, *JHEP* **03** (2010) 080 [[0911.1120](#)].
- [41] C. E. Yaguna, *The Singlet Scalar as FIMP Dark Matter*, *JHEP* **08** (2011) 060 [[1105.1654](#)].
- [42] A. Biswas and A. Gupta, *Freeze-in Production of Sterile Neutrino Dark Matter in $U(1)_{B-L}$ Model*, *JCAP* **1609** (2016) 044 [[1607.01469](#)].
- [43] A. Biswas, D. Borah and A. Dasgupta, *UV complete framework of freeze-in massive particle dark matter*, *Phys. Rev.* **D99** (2019) 015033 [[1805.06903](#)].
- [44] S. Peyman Zakeri, S. Mohammad Moosavi Nejad, M. Zakeri and S. Yaser Ayazi, *A Minimal Model For Two-Component FIMP Dark Matter: A Basic Search*, *Chin. Phys.* **C42** (2018) 073101 [[1801.09115](#)].
- [45] A. Dutta Banik, M. Pandey, D. Majumdar and A. Biswas, *Two component WIMP- \tilde{S} FIMP dark matter model with singlet fermion, scalar and pseudo scalar*, *Eur. Phys. J.* **C77** (2017) 657 [[1612.08621](#)].
- [46] K.-H. Tsao, *FIMP Dark Matter Freeze-in Gauge Mediation and Hidden Sector*, *J. Phys.* **G45** (2018) 075001 [[1710.06572](#)].
- [47] J. Alimena et al., *Searching for long-lived particles beyond the Standard Model at the Large Hadron Collider*, [1903.04497](#).
- [48] CMS collaboration, A. M. Sirunyan et al., *Search for long-lived particles decaying into displaced jets in proton-proton collisions at $\sqrt{s} = 13$ TeV*, *Phys. Rev.* **D99** (2019) 032011 [[1811.07991](#)].
- [49] CMS collaboration, A. M. Sirunyan et al., *Search for new particles decaying to a jet and an emerging jet*, *JHEP* **02** (2019) 179 [[1810.10069](#)].
- [50] CMS collaboration, A. M. Sirunyan et al., *Search for long-lived particles with displaced vertices in multijet events in proton-proton collisions at $\sqrt{s} = 13$ TeV*, *Phys. Rev.* **D98** (2018) 092011 [[1808.03078](#)].
- [51] CMS collaboration, A. M. Sirunyan et al., *Search for disappearing tracks as a signature of new long-lived particles in proton-proton collisions at $\sqrt{s} = 13$ TeV*, *JHEP* **08** (2018) 016 [[1804.07321](#)].
- [52] CMS collaboration, A. M. Sirunyan et al., *Search for long-lived particles using nonprompt jets and missing transverse momentum with proton-proton collisions at $\sqrt{s} = 13$ TeV*, [1906.06441](#).
- [53] CMS collaboration, V. Khachatryan et al., *Search for long-lived charged particles in proton-proton collisions at $\sqrt{s} = 13$ TeV*, *Phys. Rev.* **D94** (2016) 112004 [[1609.08382](#)].
- [54] ATLAS collaboration, M. Aaboud et al., *Search for long-lived neutral particles in pp collisions at $\sqrt{s} = 13$ TeV that decay into displaced hadronic jets in the ATLAS calorimeter*, [1902.03094](#).
- [55] ATLAS collaboration, M. Aaboud et al., *Search for heavy charged long-lived particles in the ATLAS detector in 31.6 fb^{-1} of proton-proton collision data at $\sqrt{s} = 13$ TeV*, [1902.01636](#).
- [56] ATLAS collaboration, M. Aaboud et al., *Search for heavy charged long-lived particles in proton-proton collisions at $\sqrt{s} = 13$ TeV using an ionisation measurement with the ATLAS detector*, *Phys. Lett.* **B788** (2019) 96 [[1808.04095](#)].
- [57] ATLAS collaboration, M. Aaboud et al., *Search for heavy long-lived multicharged particles in proton-proton collisions at $\sqrt{s} = 13$ TeV using the ATLAS detector*, *Phys. Rev.* **D99** (2019) 052003 [[1812.03673](#)].
- [58] ATLAS collaboration, M. Aaboud et al., *Search for long-lived particles produced in pp collisions at $\sqrt{s} = 13$ TeV that decay into displaced hadronic jets in the ATLAS muon spectrometer*, *Phys. Rev.* **D99** (2019) 052005 [[1811.07370](#)].

- [59] ATLAS collaboration, M. Aaboud et al., *Search for the production of a long-lived neutral particle decaying within the ATLAS hadronic calorimeter in association with a Z boson from pp collisions at $\sqrt{s} = 13$ TeV*, Submitted to: *Phys. Rev. Lett.* (2018) [[1811.02542](#)].
- [60] ATLAS collaboration, M. Aaboud et al., *Search for long-lived charginos based on a disappearing-track signature in pp collisions at $\sqrt{s} = 13$ TeV with the ATLAS detector*, *JHEP* **06** (2018) 022 [[1712.02118](#)].
- [61] LHCb collaboration, R. Aaij et al., *Updated search for long-lived particles decaying to jet pairs*, *Eur. Phys. J. C* **77** (2017) 812 [[1705.07332](#)].
- [62] LHCb collaboration, R. Aaij et al., *Search for massive long-lived particles decaying semileptonically in the LHCb detector*, *Eur. Phys. J. C* **77** (2017) 224 [[1612.00945](#)].
- [63] J. Liu, Z. Liu and L.-T. Wang, *Long-lived particles at the LHC: catching them in time*, *Phys. Rev. Lett.* **122** (2019) 131801 [[1805.05957](#)].
- [64] N. Arkani-Hamed, S. Dimopoulos and G. R. Dvali, *The Hierarchy problem and new dimensions at a millimeter*, *Phys. Lett. B* **429** (1998) 263 [[hep-ph/9803315](#)].
- [65] M. Fairbairn, A. C. Kraan, D. A. Milstead, T. Sjostrand, P. Z. Skands and T. Sloan, *Stable massive particles at colliders*, *Phys. Rept.* **438** (2007) 1 [[hep-ph/0611040](#)].
- [66] G. F. Giudice and R. Rattazzi, *Theories with gauge mediated supersymmetry breaking*, *Phys. Rept.* **322** (1999) 419 [[hep-ph/9801271](#)].
- [67] J. L. Hewett, B. Lillie, M. Masip and T. G. Rizzo, *Signatures of long-lived gluinos in split supersymmetry*, *JHEP* **09** (2004) 070 [[hep-ph/0408248](#)].
- [68] S. Banerjee, G. Bärlanger, B. Mukhopadhyaya and P. D. Serpico, *Signatures of sneutrino dark matter in an extension of the CMSSM*, *JHEP* **07** (2016) 095 [[1603.08834](#)].
- [69] N. Nagata, H. Otono and S. Shirai, *Cornering Compressed Gluino at the LHC*, *JHEP* **03** (2017) 025 [[1701.07664](#)].
- [70] S. Banerjee, G. Bärlanger, A. Ghosh and B. Mukhopadhyaya, *Long-lived stau, sneutrino dark matter and right-slepton spectrum*, *JHEP* **09** (2018) 143 [[1806.04488](#)].
- [71] L. A. Harland-Lang, V. A. Khoze, M. G. Ryskin and M. Tasevsky, *LHC Searches for Dark Matter in Compressed Mass Scenarios: Challenges in the Forward Proton Mode*, *JHEP* **04** (2019) 010 [[1812.04886](#)].
- [72] G. Cottin, J. C. Helo and M. Hirsch, *Searches for light sterile neutrinos with multitrack displaced vertices*, *Phys. Rev. D* **97** (2018) 055025 [[1801.02734](#)].
- [73] M. Drewes and J. Hajer, *Heavy Neutrinos in displaced vertex searches at the LHC and HL-LHC*, [1903.06100](#).
- [74] Y. Cui and B. Shuve, *Probing Baryogenesis with Displaced Vertices at the LHC*, *JHEP* **02** (2015) 049 [[1409.6729](#)].
- [75] K.-Y. Choi, S. K. Kang and J. Kim, *Non-thermal WIMP baryogenesis*, *Phys. Lett. B* **782** (2018) 657 [[1803.00820](#)].
- [76] X. Cid Vidal et al., *Beyond the Standard Model Physics at the HL-LHC and HE-LHC*, [1812.07831](#).
- [77] D. W. Kang and S. C. Park, *Timing information at HL-LHC: Complete determination of masses of Dark Matter and Long lived particle*, [1903.05825](#).
- [78] A. Aboubrahim and P. Nath, *Detecting hidden sector dark matter at HL-LHC and HE-LHC via long-lived stau decays*, *Phys. Rev. D* **99** (2019) 055037 [[1902.05538](#)].
- [79] D. Curtin et al., *Long-Lived Particles at the Energy Frontier: The MATHUSLA Physics Case*, [1806.07396](#).

- [80] MATHUSLA collaboration, H. Lubatti et al., *MATHUSLA: A Detector Proposal to Explore the Lifetime Frontier at the HL-LHC*, 2019, [1901.04040](#), <http://mathusla.web.cern.ch>.
- [81] G. Belanger et al., *LHC-friendly minimal freeze-in models*, [1811.05478](#).
- [82] N. Desai, *Collider signatures for dark matter and long-lived particles with Pythia 8*, [1807.04240](#).
- [83] A. Ghosh, T. Mondal and B. Mukhopadhyaya, *Heavy stable charged tracks as signatures of non-thermal dark matter at the lhc: a study in some non-supersymmetric scenarios*, *Journal of High Energy Physics* **2017** (2017) 136.
- [84] F. Jegerlehner and A. Nyffeler, *The Muon g-2*, *Phys. Rept.* **477** (2009) 1 [[0902.3360](#)].
- [85] PARTICLE DATA GROUP collaboration, M. Tanabashi et al., *Review of Particle Physics*, *Phys. Rev.* **D98** (2018) 030001.
- [86] CMS collaboration, C. Collaboration, *Searches for new phenomena in events with jets and high values of the M_{T2} variable, including signatures with disappearing tracks, in proton-proton collisions at $\sqrt{s} = 13$ TeV*, .
- [87] S. Junius, L. Lopez-Honorez and A. Mariotti, *A feeble window on leptophilic dark matter*, [1904.07513](#).
- [88] A. Alloul, N. D. Christensen, C. Degrande, C. Duhr and B. Fuks, *FeynRules 2.0 - A complete toolbox for tree-level phenomenology*, *Comput. Phys. Commun.* **185** (2014) 2250 [[1310.1921](#)].
- [89] G. B  llanger, F. Boudjema, A. Pukhov and A. Semenov, *micrOMEGAs4.1: two dark matter candidates*, *Comput. Phys. Commun.* **192** (2015) 322 [[1407.6129](#)].
- [90] K. Griest and D. Seckel, *Three exceptions in the calculation of relic abundances*, *Phys. Rev.* **D43** (1991) 3191.
- [91] L. Calibbi, L. Lopez-Honorez, S. Lowette and A. Mariotti, *Singlet-Doublet Dark Matter Freeze-in: LHC displaced signatures versus cosmology*, *JHEP* **09** (2018) 037 [[1805.04423](#)].
- [92] A. G. Hessler, A. Ibarra, E. Molinaro and S. Vogl, *Probing the scotogenic FIMP at the LHC*, *JHEP* **01** (2017) 100 [[1611.09540](#)].
- [93] J. F. Gunion, H. E. Haber, G. L. Kane and S. Dawson, *The Higgs Hunter's Guide*, *Front. Phys.* **80** (2000) 1.
- [94] A. Djouadi, *The Anatomy of electro-weak symmetry breaking. I: The Higgs boson in the standard model*, *Phys. Rept.* **457** (2008) 1 [[hep-ph/0503172](#)].
- [95] J. Herrero-Garcia, E. Molinaro and M. A. Schmidt, *Dark matter direct detection of a fermionic singlet at one loop*, *Eur. Phys. J.* **C78** (2018) 471 [[1803.05660](#)].
- [96] W. Chao, *Direct detections of Majorana dark matter in vector portal*, *JHEP* **11** (2019) 013 [[1904.09785](#)].